Quaternary Science Reviews 117 (2015) 135–151

Contents lists available at ScienceDirect

Quaternary Science Reviews

journal homepage: www.elsevier.com/locate/quascirev

On the discovery of a cave lion from the Malyi Anyui River (Chukotka, Russia)

I.V. Kirillova [a, *], A.V. Tiunov [b], V.A. Levchenko [c], O.F. Chernova [b], V.G. Yudin [d], F. Bertuch [c], F.K. Shidlovskiy [a]

[a] Ice Age Museum, "National Alliance of Shidlovskiy "Ice Age", 119 bld, Mira pr, Moscow, 129223, Russia
[b] Severtsov Institute of Ecology and Evolution, Russian Academy of Sciences, Leninskii pr. 33, Moscow, 119071, Russia
[c] Australian Nuclear Science and Technology Organisation, Locked Bag 2001, Kirrawee DC, NSW 2232, Australia
[d] Institute of Biology and Soil Science Far Eastern Branch, Russian Academy of Sciences, pr. Stoletiya Vladivostoka, 159, Vladivostok, 690022, Russia

ARTICLE INFO

Article history:
Received 10 December 2014
Received in revised form
30 March 2015
Accepted 31 March 2015
Available online 29 April 2015

Keywords:
Cave lion
Skeleton
Chukotka
Diet

ABSTRACT

An incomplete postcranial skeleton (67 elements) of a cave lion, a lower jaw and a bundle of fine yellowish hair were found by a local resident in 2008 and 2009 washed out from the perennially frozen Pleistocene sediments in the lower reaches of the Malyi Anyui River (western Chukotka). This is the first skeleton of a cave lion (*Panthera spelaea* Goldfuss) to be found in Russia. The bone sizes are similar to finds of cave lion bones known from N–E Russia, but larger than East Beringian and smaller than West European ones. The remains have been studied using a variety of methods, including morphology, morphometry, SEM-examination, AMS-dating, and isotopic study, which included examination of over 100 samples of various members of the mammoth faunal assemblage (mammoth, wooly rhinoceros, bison, horse, bear, etc.). The results showed that the northeastern Asian cave lion hunted mainly bison and horses, but not reindeer, unlike its Western Europe counterpart. Bone and claw sheath dating showed an unexpectedly old geochronological age of over 61,000 years (OZQ290, OZQ291), while the hair was dated 28,690 ± 130 (OZQ292), which makes its affinity with the same individual as the skeleton questionable. Further studies to investigate possible unremoved contamination and obtain more reliable date are planned.
© 2015 Elsevier Ltd. All rights reserved.

1. Introduction

Ex ungue leonem pingere (Latin): from the claw we may judge the lion.

In the summer of 2008, Leo Meskhe from the village of Anyuisk (Bilibino District of the Chukchi Autonomous Region) found a compact accumulation of fossil remains (67 items) 14 km upstream of Anuisk (68.18°N, 161.44°E) in a steep river bank (Fig. 1) below the water level.

From the curved claw phalanx covered by cornified sheath, the collector recognized the remains as belonging to the cave lion.

The river was washing out the mud-covered bones, which were arranged in a compact set, similar to an anatomic arrangement, with the ribs and spine visible, the latter oriented along the river-bank over about 1 m length. The limb bones were moved away from the main skeleton by the river current, and were located in the water using a testing rod. Fine mesh of metal wire was positioned downstream from the find to prevent any bones and associated objects being washed away by the river. The netted samples among others included a rounded horse vertebra and a bundle of red hair, which did not resemble the hair of an ungulate and looks more like a carnivorous fur. Remains of keratin skin derivatives of the cave lion have not previously been found. A year later, examination of the same site revealed two mandibles of the cave lion. The color and the preservation of all collected bones, as well as the anatomical structure indicated of belonging to the same individual.

The site of this locality is known as the Krasivoe Section (Mikhalev et al., 2006; Nikolaev et al., 2010), was studied for the first time by a PNIIS expedition in 1973 (Kaplina et al., 1978), and was re-examined in 1977–86 by the Northern Expedition of the Geography Faculty of Moscow State University (Arkhangelov and Konyakhin, 1978; Mikhalev, 1990). The river erosion exposed deposits of an accumulative surface 15–17 m high, which are mainly composed of frozen silt with ice lenses and ice wedge polygons. Large turf lenses up to 2–3 m thick and several meters long can be observed in the upper part of the section. The ^{14}C dating for the

* Corresponding author.
E-mail address: ikirillova@yandex.ru (I.V. Kirillova).

http://dx.doi.org/10.1016/j.quascirev.2015.03.029
0277-3791/© 2015 Elsevier Ltd. All rights reserved.

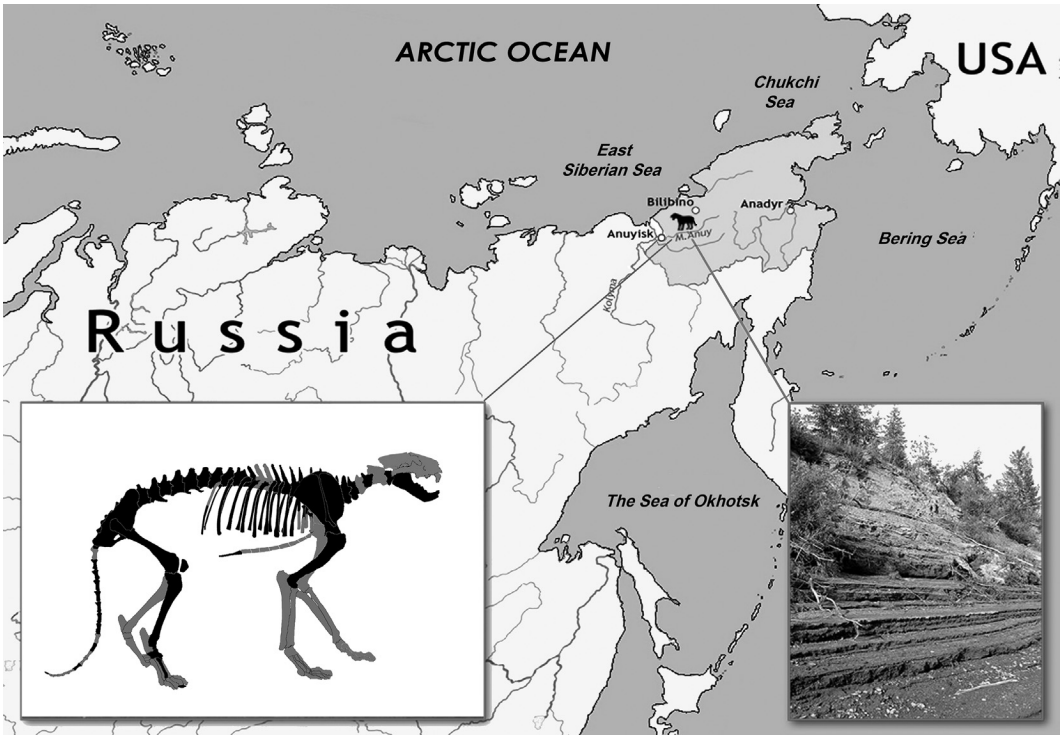

Fig. 1. Map showing the locality site. The right inset shows a stepped slope of the floodplain (the height of the upper step cutting into the slope reaches 6–7 m). The right bank of the Malyi Anyui River (Chukotka, Russia). The left inset show the composition of the Anyui lion skeleton. Preserved bones are shown in black. Collection no. F-2678/1-69. Ice Age Museum.

lower part of the section gave 27,300 ± 300 (GIN-3209) radiocarbon years, which corresponds to the Sartanian and is supported by the structural and isotope study of the ice wedges and palynological data (Tomskaya, 1982; Sher and Plaht, 1988; Konyakhin et al., 1996; Mikhalev et al., 2006).

Like other rivers of northeastern Russia, the floodplain of the Malyi Anyui River has a distinct micro-terraced topography, which is developed in the lower riverbank at the interval of about 7 m above the low water level (Fig. 1, right inset). This structure is produced by water level after spring flood dropping in stages of 5–10 to 30 cm, with erosion forming a step in loose deposits of riverbank at each intermediate water level.

The cave lion skeleton was found on the one of such freshly cut micro-terraces.

2. Material

(1) Cave lion skeleton F-2678/1-69, incomplete (Fig. 1, left) from right bank in the lower reaches of the Malyi Anyui river. The skeleton recovered includes 69 bones: 2 branches of the mandibulae – 2; vertebrae – 34; ribs – 20; corpus sternum – 1; scapula – 1; humerus – 1; coxae – 2; patellae – 2; femur – 1; tibia – 1; fibula – 1; III metatarsus – 1; astragalus – 1; phalanx III with a claw sheath – 1. Bones are in different state of preservation (from moderate to excellent).

(2) Cave lion remains from N–E Russia, previously unpublished: F-150, F-279, F-2450 (mandibles); F-2879 (atlas); F-755a (humerus).

(3) Analytical probes of animal remains (cave lion, canids, bear, mammoth, wooly rhinoceros, deer, bison, horse, and bighorn sheep) from northeastern Russia. A list of a total of 100 probes and the results of the isotope study are discussed in the section "Results" (Table 1).

The materials are kept in the Ice Age Museum (Shidlovskiy's National Alliance "Ice Age"), Russia.

3. Methods

3.1. Bone measurement and individual age estimation

We follow the taxonomy of Sotnikova and Nikolsky (2006) for the cave lion, and treat it as a full species *Panthera spelaea* Goldfuss.

The cave lion mandibles were measured using digital calipers SHCC-1-300 and SHCC-1-500, with an accuracy of better than 0.1 mm. von den Driesch's (1976) system of measurements and abbreviations was used. The radiographic imaging of the left side of the lower jaw was performed in the veterinary clinic "Sopiko" (Moscow) using the Sedecal APR-VET system. Measurements of the rest of the bones were taken with the measurement box with 0.5 mm accuracy again following von den Driesch's (1976) methodology.

The right canine, split longitudinally along the natural fractures, was strengthened using polyvinyl butyral resin (PVB), and its root was sectioned transversally. These surfaces (longitudinal polished section and transverse thin section) were studied in reflected light using a Leica StereoZoom 6 light Microscope. The age of the canine was calculated using the layers of cement on the longitudinal and transverse sections using Klevezal's (1988) protocol.

3.2. Geological Age determination

Geological Age determination was performed on three different samples – bone (rib), claw sheath and hair/wool – by radiocarbon AMS at the Australian Nuclear Science and Technology Organisation (ANSTO) on the STAR AMS 2 MV Tandetron on graphite targets (Fink et al., 2004). To remove possible contamination the samples

Table 1
A list of samples of mammalian tissues from the mammoth faunal assemblage, and results of stable isotope analysis. Note 1. Sample F-150 was impregnated with polyvinyl butyral glue (BF-2).

Species	Region	Site	Specimen no.	Skeletal element (bone collagen) or tissue	%C	%N	Atom C/N	$\delta^{13}C$ (‰)	$\delta^{15}N$ (‰)
Panthera spelaea	Chukchi Peninsula	Malyi Anyui River	F-2678/48	Costa	46.6	17.1	3.2	−19.9	12.6
		Malyi Anyui River	F-2678/118	Costa	45.8	16.6	3.2	−19.8	12.5
		Malyi Anyui River	F-2678/119	Pelvis	47.2	17.0	3.2	−19.9	12.5
		Malyi Anyui River	F-2678/120	Vertebra	45.7	16.6	3.2	−19.9	12.5
		Malyi Anyui River	F-2678/69	Mandibula	48.0	17.7	3.2	−19.2	11.4
		Malyi Anyui River	F-2450	Mandibula	45.4	16.6	3.2	−19.0	9.6
		Malyi Anyui River	F-2678	Hair	46.9	15.4	3.5	−21.2	12.0
		Malyi Anyui River	F-2678	Hair	44.6	14.4	3.6	−21.3	12.1
		Malyi Anyui River	F-2678	Hair	44.7	13.9	3.8	−21.7	12.1
		Malyi Anyui River	F-2678	Claw	43.3	13.7	3.7	−21.4	11.6
		Malyi Anyui River	F-2678	Claw	41.1	13.1	3.6	−21.1	11.8
Panthera spelaea	Yakutia	Alazeya River, village Andryushkino	F-2651	Cranium	44.7	16.3	3.2	−20.4	11.8
		Duvanny Yar, Lower Kolyma	F-2671	Maxilla	46.9	17.2	3.2	−19.1	12.0
		Duvanny Yar, Lower Kolyma	F-278	Cranium	47.4	17.2	3.2	−20.2	12.0
		Lower Kolyma	F-150	Mandibula	46.9	16.8	3.3	−19.8	12.4
Ursus	Chukchi Peninsula	Pogindina river, tributary of Malyi Anyui River	F-2374	Humerus	45.8	16.9	3.2	−19.6	12.3
		Pogindina river, tributary of Malyi Anyui River	F-2723	Cranium	43.0	15.7	3.2	−20.2	9.0
Ursus	Yakutia	Alazea river	F-931	Sacrum	45.8	16.8	3.2	−19.0	12.8
		Terekhtyakh river	F-2296	Humerus	45.2	16.5	3.2	−20.1	11.8
Canis sp.	Chukchi Peninsula	Malyi Anyui River, 14–25 km upstream of Anyuisk settlement	F-2449	Cranium	43.9	16.0	3.2	−20.1	10.3
Canis sp.	Yakutia	Alazeya River, village Andryushkino	F-945	Cranium	46.3	17.1	3.2	−21.1	10.7
		Alazeya River	F-2672	Cranium	47.5	17.2	3.2	−20.0	13.3
		Alazeya River, village Andryushkino	F-933	Mandibula	47.6	17.4	3.2	−19.6	11.2
		North-East Yakutia	No number	Cranium	47.9	17.7	3.2	−19.9	9.7
		Letnyaya River	F-3055	Cranium	47.5	17.6	3.1	−19.1	12.9
		Letnyaya River	F-3056	Tibia	46.3	16.9	3.2	−20.9	9.9
Mammuthus	Chukchi Peninsula	Anyuisk settlement	No number	Vertebra	40.0	14.8	3.2	−20.9	12.0
		Malyi Anyui River, 14–25 km upstream of Anyuisk settlement	F-3044	Humerus	45.8	16.1	3.3	−21.0	9.5
		Malyi Anyui River, 14–25 km upstream of Anyuisk settlement	F-1885	Cranium	47.2	17.1	3.2	−21.7	9.6
		Malyi Anyui River, 14–25 km upstream of Anyuisk settlement	F-1915	Humerus	46.1	17.0	3.2	−21.6	9.1
		Malyi. Anyui River, 14–25 km upstream of Anyuisk settlement	F-3040	Vertebra	45.9	16.7	3.2	−21.8	9.7
		Anyuisk settlement	F-3030	Femur	46.8	17.2	3.2	−21.5	9.9
		Coast of the East Siberian Sea	F-2403	Scapula	46.2	16.9	3.2	−22.0	10.0
		Malyi Anyui River, 14–25 km upstream of Anyuisk settlement	F-3043	Atlas	45.4	16.6	3.2	−20.7	7.9
		Coast of the East Siberian Sea	F-2402	Scapula	45.6	16.7	3.2	−21.3	7.7
		Malyi Anyui River, 14–25 km upstream of Anyuisk settlement	F-3045	Femur	46.1	16.7	3.2	−22.1	10.2
Mammuthus	Yakutia	Rassokha River	F-2757/35	Costa	46.0	16.7	3.2	−22.3	11.0
		Beryozovka River	F-3034	Cranium	47.7	17.3	3.2	−21.4	10.8
		North of Kolyma Lowland	F-2398	Ulna	46.2	16.9	3.2	−21.4	8.7
		Chondon River	F-768	Tibia	47.2	17.4	3.2	−21.4	9.9
		Beryozovka River	F-300/1	Cranium	44.6	16.4	3.2	−21.4	10.8
		Panteleikha River	F-604	Ulna	45.3	16.3	3.2	−21.5	7.7
		Panteleikha River	F-600	Ulna	44.0	16.0	3.2	−21.8	9.2
Mammuthus	Taymyr	Kastykhtakh river	F-2644	Cranium	46.8	16.7	3.3	−22.3	9.3
Coelodonta	Chukchi Peninsula	Malyi Anyui River, 14–25 km upstream of Anyuisk settlement	F-2944	Mandibula	45.0	16.5	3.2	−20.6	7.6
		Malyi. Anyui River, 14–25 km upstream of Anyuisk settlement	F-2927	Scapula	46.7	17.1	3.2	−20.9	8.2
		Malyi Anyui River, 14–25 km upstream of Anyuisk settlement	F-2946	Cranium	46.1	16.8	3.2	−20.5	8.5
		Malyi Anyui River, 14–25 km upstream of Anyuisk settlement	F-2941	Pelvis or femur	47.7	17.3	3.2	−21.0	10.8
		Malyi Anyui River, 14–25 km upstream of Anyuisk settlement	F-2956	Metapodia	47.9	17.4	3.2	−20.9	8.2
		Malyi Anyui River, 14–25 km upstream of Anyuisk settlement	F-2945	Tibia	46.9	17.1	3.2	−20.8	5.2
		Malyi Anyui River, 14–25 km upstream of Anyuisk settlement	F-2960	Radius	47.4	17.1	3.2	−21.0	9.1
		Malyi Anyui River, 14–25 km upstream of Anyuisk settlement	F-2940-2	Pelvis	47.8	17.5	3.2	−20.5	9.2
		Malyi Anyui River, 14–25 km upstream of Anyuisk settlement	F-2963	Tibia	46.8	17.2	3.2	−20.9	6.0
			F-2928	Scapula	47.0	17.2	3.2	−20.8	9.7

(*continued on next page*)

Table 1 (*continued*)

Species	Region	Site	Specimen no.	Skeletal element (bone collagen) or tissue	%C	%N	Atom C/N	$\delta^{13}C$ (‰)	$\delta^{15}N$ (‰)
		Malyi Anyui River, 14–25 km upstream of Anyuisk settlement							
		Malyi Anyui River, 14–25 km upstream of Anyuisk settlement	F-2954	Radius	44.9	16.5	3.2	−21.4	10.1
		Malyi Anyui River, 14–25 km upstream of Anyuisk settlement	F-2957	Radius	45.3	16.5	3.2	−20.4	10.0
		Malyi Anyui River, 14–25 km upstream of Anyuisk settlement	F-2961	Radius	42.9	15.7	3.2	−20.7	7.7
		Malyi Anyui River, 14–25 km upstream of Anyuisk settlement	F-2962	Radius	46.2	16.9	3.2	−20.6	7.2
Equus	Chukchi Peninsula	Malyi Anyui River, 14–25 km upstream of Anyuisk settlement	F-2993	Vertebra	46.6	17.0	3.2	−21.1	6.7
		Malyi Anyui River, 14–25 km upstream of Anyuisk settlement	F-2988	Mandibula	47.2	17.1	3.2	−20.9	6.6
		Malyi Anyui River, 14–25 km upstream of Anyuisk settlement	F-2979	Metatarsale	45.0	16.3	3.2	−21.3	5.4
		Malyi Anyui River, 14–25 km upstream of Anyuisk settlement	F-2987	Cranium	46.5	16.8	3.2	−21.2	6.2
		Malyi Anyui River, 14–25 km upstream of Anyuisk settlement	F-2982	Metatarsale	46.4	17.0	3.2	−21.0	5.8
		Malyi. Anyui River, 14–25 km upstream of Anyuisk settlement	F-2972	Tibia	47.1	17.2	3.2	−21.0	5.9
		Malyi Anyui River, 14–25 km upstream of Anyuisk settlement	F-2989	Mandibula	46.4	16.8	3.2	−21.3	6.1
		Malyi Anyui River, 14–25 km upstream of Anyuisk settlement	F-2990	Mandibula	47.6	17.0	3.3	−21.0	3.7
		Malyi Anyui River, 14–25 km upstream of Anyuisk settlement	F-2977	Metatarsale	47.2	17.2	3.2	−20.7	5.5
		Malyi Anyui River, 14–25 km upstream of Anyuisk settlement	F-3002	Humerus	46.9	17.2	3.2	−21.1	7.7
		Malyi Anyui River, 14–25 km upstream of Anyuisk settlement	F-2969	Femur	46.0	17.0	3.2	−20.5	7.7
		Malyi Anyui River, 14–25 km upstream of Anyuisk settlement	F-2971	Femur	45.9	16.9	3.2	−21.1	6.6
		Malyi Anyui River, 14–25 km upstream of Anyuisk settlement	F-2976	Tibia	45.8	16.8	3.2	−22.0	9.0
		Malyi Anyui River, 14–25 km upstream of Anyuisk settlement	F-2968	Pelvis	47.0	17.2	3.2	−21.1	5.6
		Malyi Anyui River, 14–25 km upstream of Anyuisk settlement	F-2974	Tibia	46.9	17.2	3.2	−20.9	5.9
		Malyi Anyui River, 14–25 km upstream of Anyuisk settlement	F-2967	Pelvis	45.8	16.8	3.2	−21.1	5.5
		Malyi Anyui River, 14–25 km upstream of Anyuisk settlement	F-2970	Femur	47.4	17.4	3.2	−20.7	8.9
Equus	Yakutia	Letnyaya River	F-3058	Radius	47.8	17.0	3.3	−22.0	6.9
		Letnyaya River	F-3059	Radius	46.1	17.0	3.2	−20.8	8.9
Rangifer	Chukchi Peninsula	Malyi Anyui river, 14–25 km upstream of Anyuisk settlement	F-3027	Cranium	46.1	16.9	3.2	−17.9	4.5
		Malyi Anyui river, 14–25 km upstream of Anyuisk settlement	F-3027	Antler	42.4	15.2	3.2	−18.9	5.4
		Malyi Anyui river, 14–25 km upstream of Anyuisk settlement	F-3025	Cranium	44.5	16.2	3.2	−19.7	3.3
		Malyi Anyui river, 14–25 km upstream of Anyuisk settlement	F-3025	Antler	46.6	17.2	3.2	−20.3	5.7
		Malyi Anyui river, 14–25 km upstream of Anyuisk settlement	F-3029	Metacarpale	46.2	17.0	3.2	−19.5	7.0
		Malyi Anyui river, 14–25 km upstream of Anyuisk settlement	F-3024	Vertebra	48.6	18.0	3.2	−20.7	7.8
		Anyuisk settlement	no number	Cranium	43.8	15.9	3.2	−19.4	4.7
		Pogindina river, tributary of Malyi Anyui River	F-2373	Mandibula	44.4	16.3	3.2	−19.4	6.9
Rangifer	Yakutia	Letnyaya River	F-3066	Cranium	44.0	16.2	3.2	−20.5	7.9
		Letnyaya River	F-3065	Cranium	47.4	17.5	3.2	−19.2	1.7
		Letnyaya River	F-3065	Antler	45.2	16.7	3.2	−19.7	1.9
Cervus	Chukchi Peninsula	Rauchua River	F-3032	Antler	47.4	17.3	3.2	−20.0	5.7
		Anyuisk settlement	F-3123	Antler	44.8	16.4	3.2	−19.8	4.5
		Anyuisk settlement	F-3124	Antler	45.0	15.9	3.3	−19.5	3.8
Bison	Chukchi Peninsula	Rauchua River mouth	F-3246-5	Costa	48.1	17.2	3.3	−21.9	8.0
		Rauchua River mouth	F-3246-116	Costa	43.9	15.9	3.2	−21.3	7.7
		Rauchua River mouth	F-3246-117	Vertebra	45.5	16.4	3.2	−21.3	7.7
		Anyuisk settlement	F-3080	Cranium	44.6	16.4	3.2	−21.0	6.4
		Anyuisk settlement	F-3079	Cranium	44.9	16.5	3.2	−20.8	8.3
		Anyuisk settlement	F-3077-1	Cranium	44.6	16.4	3.2	−20.7	7.2
			F-3009	Metacarpale	45.8	16.8	3.2	−21.4	7.1

Table 1 (*continued*)

Species	Region	Site	Specimen no.	Skeletal element (bone collagen) or tissue	%C	%N	Atom C/N	$\delta^{13}C$ (‰)	$\delta^{15}N$ (‰)
		Malyi Anyui river, 14–25 km higher Anyuisk settlement							
		Malyi Anyui river, 14–25 km higher Anyuisk settlement	F-3010	Radius	46.9	17.0	3.2	−20.9	7.8
		Malyi Anyui river, 14–25 km higher Anyuisk settlement	F-3008	Metacarpale	46.2	16.7	3.2	−21.3	5.6
		Malyi Anyui river, 14–25 km higher Anyuisk settlement	F-3011	Cranium	45.0	16.3	3.2	−21.5	7.5
Bison	Yakutia	Letnyaya River	F-3076	Phalanx I	43.1	15.7	3.2	−20.9	8.0
		Alazeya River basin	F-2884-3	Metatarsale	48.7	17.8	3.2	−21.3	7.6
Ovibovini	Chukchi Peninsula	Malyi Anyui river, 14–25 km higher Anyuisk settlement	F-3001	Cranium	45.5	16.7	3.2	−20.8	5.5
		Malyi Anyui river, 14–25 km higher Anyuisk settlement	F-3000	Cranium	46.8	17.0	3.2	−20.4	8.0
		Pogindina river, tributary of Malyi Anyui River	F-2372	Cranium	44.8	16.4	3.2	−20.3	6.4
Ovibovini	Yakutia	Indigirka River	F-225	Mandibula	40.9	14.9	3.2	−20.6	6.9
Ovis nivicola	Chukchi Peninsula	Mandrikovo settlement	F-2636	Cranium	47.1	17.3	3.2	−20.3	8.0

OZQ291 (claw) and OZQ292 (wool/hair) were treated following the O'Connell and Hedges (1999) protocol. It included ultra-sonication first in deionized water, then twice in a mixture of methanol and chloroform, and finally three times in deionized water again. The samples were then treated with 2M HCl at room temperature for 2 h to remove any carbonate contamination and then rinsed with deionized water. The samples were then freeze-dried and processed to graphite following Hua et al. (2001).

Collagen was extracted from the bone sample for radiocarbon dating using the ultrafiltration protocol (Brown et al., 1988; Higham et al., 2006) of bone sample pretreatment. The ultrafiltration method, which acts to remove material with a molecular weight below 30 kD including salts, fulvic acids and degraded collagen, has been shown to remove contamination more effectively than other methods (Bronk Ramsey et al., 2004). A series of quality control tests to assess the suitability of the extracted collagen and claw keratin were done on sample aliquots with EA-IRMS (Elementar varioMICRO CUBE coupled to a Micromass Isoprime); results are presented below.

The hair/wool sample, because of its small size, was not subjected to these tests.

3.3. Stable isotope composition determination

Samples of bone tissue were obtained using a bone-cutting drill. Collagen was extracted using a modified Longin (1971) method. Bone or antler fragments (typically 0.5–1 g) were sampled from faunal specimens. Any visible foreign material was removed with a brush. Samples were then washed, dried and weighed. Bone fragments were soaked in 1 M HCl until they were completely demineralized. Samples were then rinsed to neutrality with distilled water, leaving the insoluble collagen in a slightly acidic solution (pH ~ 2.5). The solution containing the insoluble residue was heated in plastic tubes at 90 °C for 24–36 h to gelatinize the collagen. Samples were then centrifuged and the gelatinized collagen was transferred into glass vials. Vials were placed in a sealed oven until all water was evaporated at 80 °C. The extracted collagen was then transferred into tin cups for isotopic analysis. One sample of cave lion bone was fixed with butylphenol formaldehyde resin. The influence of resin on isotopic composition is still unclear, so this result should be used with caution (Lopez-Polin, 2012). Samples of hair and claw were degreased with alcohol, thoroughly washed with distilled water and dried.

OZ number	Client ID	Collagen %	C:N (atomic)	$\delta^{13}C$	$\delta^{15}N$
Q290	S-2 – F-2678/48 rib	15.4	3.3	−20.10 ± 0.1	12.5 ± 0.1
Q291	S-3 – F-2678/66 claw	–	3.6	−20.7 ± 0.1	12.8 ± 0.1

At 15.4% collagen yield, sample OZQ290 exhibited excellent quality collagen which is consistent with its preservation in permafrost. The atomic C:N ratio of the collagen and keratin lies within the normal range indicating that the preservation of the material was acceptable for dating, and contaminants had been effectively removed. Keratin, as expected, exhibited slightly higher C:N ratio than collagen (O'Connell et al., 2001). Isotopic measurements also produced values within acceptable ranges, confirming the suitability of material for radiocarbon dating (van Klinken, 1999).

Once the collagen has been extracted the samples were processed to graphite in the AMS chemistry laboratories (Hua et al., 2001). Determinations of $\delta^{13}C$ for the purposes of isotopic fractionation correction were done on the residue of graphite targets, derived from the studied chemical fraction after the radiocarbon AMS measurement was completed. Measurements were again performed on the same EA-IRMS.

Stable isotope composition of bone collagen and keratin was determined using a Thermo-Finnigan Delta V Plus continuous-flow IRMS coupled with an elemental analyzer (Thermo Flash 1112) in the Joint Usage Center at the Institute of Ecology and Evolution RAS. The isotopic composition of N and C was expressed in the δ-notation relative to the international standard (atmospheric nitrogen or VPDB): $\delta X(‰) = [(R_{sample}/R_{standard}) - 1] \times 1000$, where R is the ratio of the heavier isotope to the lighter isotope. Samples were analyzed with reference gas calibrated against IAEA reference materials USGS 40 and USGS 41 (glutamic acid). The drift was corrected using an internal laboratory standard (acetanilide). The standard deviation of $\delta^{13}C$ and $\delta^{15}N$ values in USGS 40 ($n = 8$) was <0.2‰. Along with isotopic analyses, nitrogen and carbon contents (as %) were determined for all samples.

Traces on the canine are studied using an MBS-10 binocular microscope and photographed under a Keyence VHX-1000 digital microscope.

4. Results

4.1. Description and measurement of bones

4.1.1. Axial skeleton

Right mandible, F-2678/68 (Fig. 2C). The bone is complete. The incisors are missing. The right canine, p4 and m1 are preserved. The anterior edge of the m1 is slightly behind the posterior edge of p4, deforming the dental arch. The pm is noticeably turned along the vertical axis with the paraconid in the lingual position and talonid in the buccal position. The surface of the bone on the lingual side on the os dentale is noticeably nodular, especially under the tooth row. Foramina are considerably enlarged around the m1, p4, canine and on the symphisial side. Small osteophytes are developed on the buccal side of the symphysis. Measurements are given in Table 2.

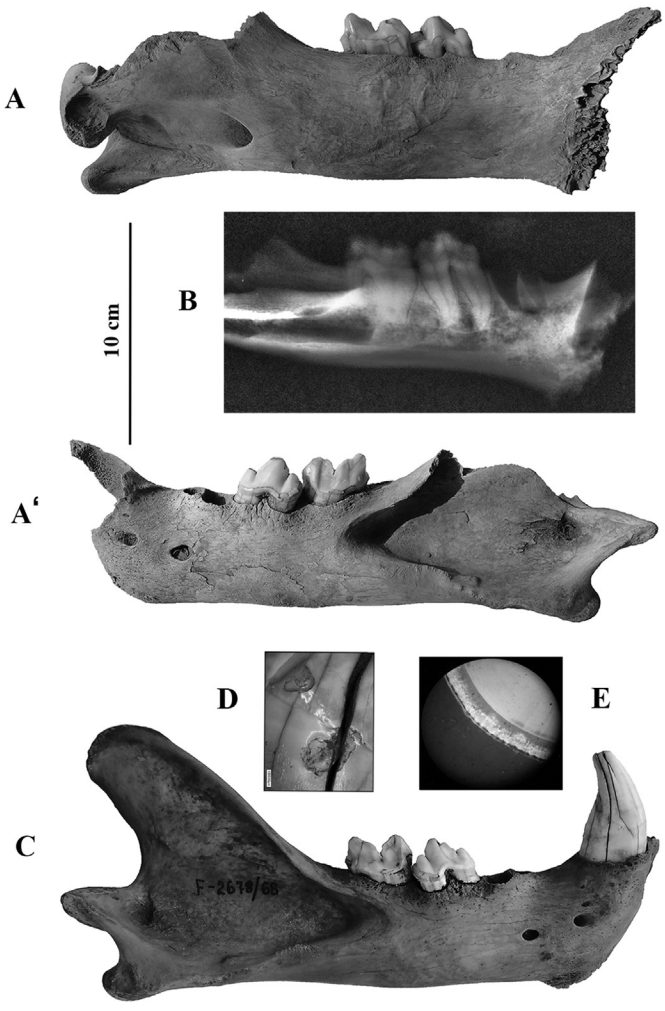

Fig. 2. Mandibles of the Anyui lion. Left mandible, F-2678/69: A — lingual view, A' — buccal view, C — radiograph. The center of the mandible shows irregular areas of denser compact bone and pathological transformation due to periostitis. Right mandible of a cave lion, F-2678/68. Note enlarged foramina on *osdentale* near the base of the teeth (early stage of age-related degeneration). C — buccal view. D — dent on canine, possibly the trace of an impact. E — transverse section of canine under the microscope. Note evenly wavy lines of annual increments of the several most recent cement layers. Ice Age Museum.

Left mandible F-2678/69. The coronoid process and part of the symphysis are broken off (Fig. 2A). A quarter of the external surface on the buccal side is damaged. The anterior edge of the m1 is slightly shifted behind the posterior edge of the p4, misaligning with the dental arch. The p4 is noticeably turned relative to the longitudinal axis of the jaw with the paraconid in the lingual position and the talonid in the buccal position. Foramina are noticeably enlarged around the m1, p4 and on the symphysis side. The lingual surface bears prominent irregularities, also visible on the X-Ray (Fig. 2A, B). The buccal surface is also uneven. The compact bone flakes off in places (Fig. 2A′).

The right canine is large, the enamel and dentine are well preserved. The tooth is slightly curved laterally. The distance from the tip of the cusp to the root base measured along a straight line is 97.7 mm. The maximum size is as follows: width/root diameter is 28.8/20.4 mm; the width/tooth diameter at the cusp base is 26.5/20.7; the maximum height of the cusp is 37.2 mm. The cusp tip was worn off during the animal's lifetime to form a surface 8.4 × 7.8 m. The pulp chamber is closed apically. The root cross-section shows that dentine does not completely fill the pulp cavity. The dentin is stained for more than a half of the tooth. The root surface shows three transverse annuli: one, clearly pronounced at a distance of 45 mm along a straight line from the cusp tip, the second, less conspicuous, but also distinct is at about 66.5 mm from the cusp tip, and the third, indistinct, is below the second. These annuli are thin layers of slow growth, usually related to cold seasons (Klevezal, 1988) in annual cycles of tooth root development.

The deep post-mortem cracks are filled by small fragments of grass, suggesting a long subsurface burial in the seasonal thaw zone (at least two warm seasons). In the middle of the inner surface immediately below the cusp there is a small (4 mm in diameter) trace left by the impact of a hard object. This injury is a dent with an uneven bottom and sides distinctly outlined on the root side and smoothened on the cusp side. The boundary between the distinct and smoothened zones is gradual. On the cusp side the smoothness, the polished finish, and linear traces are the same as on the adjacent enamel, gradually weakening toward the root. A similar, but smaller dent is near, anterior to, the one discussed above.

Vertebral column consists of 36 vertebrae, including 5 cervical vertebrae; 11 thoracic vertebrae; 7 lumbar vertebrae; 3 sacral vertebrae, and 10 caudal vertebrae. Some vertebrae have angular extensions of the rib head facets and transverse processes. Some vertebrae are asymmetrical.

Cervical vertebrae (Fig. 3). Five vertebrae are preserved. Some lateral and spinous processes are damaged. The second and the fourth vertebrae are missing.

Atlas F-2678/1 (Fig. 3-1). The tubercles of the ligaments attachment sites are prominent. The interior of the spinal canal walls at the level of the transverse processes is uneven showing a combination of natural irregularities of the bone and small dents, up to 5 mm is size. Measurements of main postcranial bones are given in Table 3.

The third cervical vertebra F-2678/2 (Fig. 3-2). The tubercles of the ligament attachment sites are prominent.

The fourth cervical vertebra F-2678/3 (Fig. 3-3). The muscle attachment areas are well developed, but less so than in the above described vertebrae. The asymmetry of the transverse processes is distinct posteriorly, which is particularly noticeable in the bottom view.

The fifth cervical vertebra F-2678/4 (Fig. 3-4). The vertebra is asymmetrical: the spinous process is somewhat inclined to the left; the inferior left process is noticeably wider than the right (the width is 33.3 and 22.2 mm, respectively); the left transverse foramen is considerably wider than the right (maximum diameters

Table 2
Measurements of cave lion mandibles (mm) from the Malyi Anyui River (F-2678/68) and comparison with other finds.

N°	Measurements	F-2678/68 ♂	F-150 ♀ Lower Kolyma	F-279 ♂ Lower Kolyma	F-2450 ♀ Maly Anuyu	N–E Russua* ♀♂		France** ♂	East Beringia***
						Middle Pleistocene	Late Pleistocene		
1	Total length (from the condyle process – Infradentale)	264.0	(204.0)	250.0	209.0	249.0–278.0	210.0–246.1	285.4	226–248♂♂ 194–215♀♀
2	Length from the indentation between the condyle process and the angular process – Infradentale	244.0	(188.0)	(238.0)	199.0	238.0–268.0	232.5–236.5	273.8	–
3	Length: the condyle process – aboral border of the canine alveolus	223.0	(179.0)	210.5	176.0	207.0–240.0	200.1–206.6	–	–
4	Length from the indentation between the condyle process and the angular process – aboral border of the canine alveolus	206.0	(167.0)	200.0	166.0	227.0–228.0	193.0–197.0	–	–
5	Length of the cheektooth row, P_3-M_1, measured along the alveoli	82.0	(72.0)	70.0	68.0	70.3–86.8	62.8–75.3	84.5	–
6	Length of M_1, measured at the cingulum	29.5	24.5	(26.0)	25.5	26.8–33.4	23.9–29.2	32.0	–
6a	Breadth of M_1, measured at the cingulum	14.5	12.0	13.5	13.8	13.0–17.3	13.0–14.6	–	
7	Length of the carnassial alveolus	29.5	27.0	27.0	26.3	27.3–35.0	26.0–30.1	–	–
8	Height of the vertical ramus: basal point of the angular process – Coronion	129.0	–	–	95.0	115.7–139.6	95.3–117.6	141.6	–
9	Height of the mandible behind M_1, measured on the buccal side	52.6	46.0	55.5	42.7	45.0–58.3	45.5–56.3	60.0	–
10	Height of the mandible in front of P3, measured on the buccal side	51.5	39.5	50.0	42.4	44.7–57.8	38.7–55.2	58.0	–

Notes. The accuracy of Malyi Anyui River sample (F-2678/68) measurements is 0.1 mm. The measurements in parentheses are made on the damaged samples.
According to: * Boeskorov et al. (2012). ** A. Argant (1988). *** B. Kurtén (1985).

posteriorly are 9.1 and 4.7 mm, anteriorly 10.6 and 4.8 mm, respectively).

The seventh cervical vertebra F-2678/5 (Fig. 3-5). The neural arch is asymmetrical. The anteroposterior measurements of the processes are 63.2 mm on the left and 53.8 on the right.

Thoracic vertebrae (Fig. 4A). The anterior thoracic vertebrae are brownish, whereas the posterior thoracic vertebrae are whitish. The eighth and the ninth thoracic vertebrae are missing.

The first thoracic vertebra F-2678/6. The neural arch possesses small osteophytes on either side. The vertebra is asymmetrical. The right articular facet for articulation with the seventh cervical vertebra is larger than the left and it is slightly more turned anteriorly than the left. The posterior facets for articulation with the second thoracic vertebra and neural arches from the vertebra body to the spinous process are also asymmetrical. The spinous process is slightly inclined to the left.

The second thoracic vertebra F-2678/7. The posterior ridge of the spinous process is slightly deformed in the lower half. The osteophytes are also located in this region. The anterior is noticeably asymmetrical.

The third and the fourth thoracic vertebra F-2678/8-9. Both vertebrae have unusual deep elongated depressions at the base of the spinous process (Fig. 4A, -3 and -4, indicated by arrows). The length of the largest depression is up to 2 cm, the width is up to 0.4 cm.

Other thoracic vertebrae have usual morphology.

Lumbar vertebrae (Fig. 5). All seven vertebrae are present (F-2678/17-23). The left transverse processes are damaged in all vertebrae, whereas the right ones are damaged on the third, fourth and partly on the seventh vertebrae. The bodies of the second thoracic vertebra posteriorly and of the third anteriorly are asymmetrical due to a slight deformation (Fig. 5 B).

Sacrum, F-2678/24 (Fig. 6 A). The sacrum is composed of three long-ago fused vertebrae, with hardly visible sutures at their points of contact. A small gap is observed between the last two vertebrae. The sacrum alae are symmetrical. The right ala is somewhat

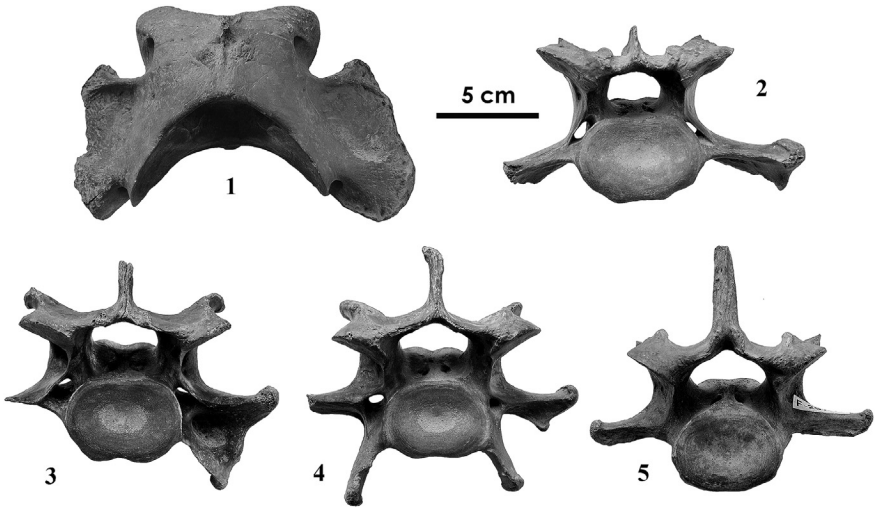

Fig. 3. Cervical vertebrae of the Anyui lion.1 — I (atlas); 2 — III; 3 — Y; 4 — YI; 5 — YII. Specimens F-2678/1-5. Ice Age Museum.

Table 3
Measurements of cave lion bones (mm) from the Malyi Anyui River (F-2678) and comparison with other finds.

	Measurements	Specimens and references			
	Atlas	**F-2678/1**	**F-2879** N–E Russia	–	–
GL	Greatest length	89.0	85.0	–	–
GB	Greatest breadth over the wings, real	(155.0)	166.0	–	–
GB	Greatest breadth over the wings, reconstructed	175.0	166.0	–	–
BFcr	(Greatest) breadth of the Facies articularis cranialis	75.5	68.0	–	–
Bfcd	(Greatest) breadth of the Facies articularis caudalis	79.0	81.0	–	–
LAd	Length of the Arcus dorsalis, median	37.0	35.0	–	–
H	Height	56.0	55.0	–	–
LAv	Length of the Arcus ventralis, median	26.0	27.0	–	–
	Sacrum, F-2678/24		–	–	–
GL	Greatest length	134.0	–	–	–
PL	Physiological length	115.0	–	–	–
GB	Greatest breadth (across the wings)	103.0	–	–	–
BFcr	(Greatest) breadth of the Facies terminalis cranialis	54.0	–	–	–
HFcr	(Greatest) height of the Facies terminalis cranialis	34.0	–	–	–
	Sternum bone, F-2678/62		–	–	–
GL	Greatest length	83.0	–	–	–
	Scapula, F-2678/55			–	–
HS	Height along the spine	326.0	–	–	–
SLC	Smallest length of the Collum scapulae (neck of the scapula)	72.0	–	–	–
GLP	Greatest length of the Processus articularis	82.0	–	–	–
	Humerus	**F-2678/56**	**F-755a** Lower Kolyma	**No number**[a]	**NW Germany**[b]
GL	Greatest length	385.0	–	(363.0)	319.0–396.0
GLC	Greatest length from caput	370.0	–	355.0	–
Bp	(Greatest) breadth of the proximal end. Not in canids	88.0	–	88.0	–
SD	Smallest breadth of diaphysis	36.5	28.0	34.5	–
Bd	(Greatest) breadth of the distal end	103.0	81.0	96.0	84.0–103.0
	Pelvis, F-2678/57				
GL	Greatest length of one half	382.0	–	–	–
LAR	Length of the acetabulum on the rim	54.0	–	–	–
LS	Length of the symphysis (only when the two halves have fused)	(140.5)	–	–	–
SH	Smallest height of the shaft of ilium	62.0	–	–	–
SB	Smallest breadth of the shaft of ilium	31.0	–	–	–
LFo	Inner Length/breadth of foramen obturatum	85.0/49.0			
	Femur	**F-2678/59**	–	–	**NW Germany**
GL	Greatest length	432.0	–	–	359.0–465.0
GLC	Greatest length from caput	428.0	–	–	–
Bp	(Greatest) breadth of the proximal end	107.0	–	–	–
DC	(Greatest) depth of the Caput femoris	48.0	–	–	–
SD	Smallest breadth of diaphysis	38.5	–	–	–
Bd	(Greatest) breadth of the distal end	92.0	–	–	77.0–96.0
	Patella, F-2678/64				
GL	Greatest length	70.0	–	–	–
GB	Greatest breadth	45.0	–	–	–
	Patella, F-2678/65				
GL	Greatest length	68.0	–	–	–
GB	Greatest breadth	46.0	–	–	–
	Tibia	**F-2678/60**	–	–	**NW Germany**
GL	Greatest length	362.0	–	–	312.0–392.0
Bp	(Greatest) breadth of the proximal end	95.0	–	–	–
SD	Smallest breadth of diaphysis	35.0	–	–	–
Bd	(Greatest) breadth of the distal end	66.0	–	–	–
Dd	(Greatest) depth of the distal end	48.0	–	–	56.0–71.0
	Fibula, F-2678/61				–
GL	Greatest length	328.0	–	–	–
	Astragal, F-2678/63				
GL	Greatest length	70.0	–	–	–
GB	Greatest breadth	57.0	–	–	–
	Metatarsal III, F-2678/67				–
GL	Greatest length	144.0	–	–	–

Notes: The accuracy of Malyi Anyui River sample (F-2678/68) measurements is 0.5 mm. The measurements given in parentheses, are made on damaged bones.
[a] The specimen without a collection number (private collection). Omolon River (right tributary of the Lower Kolyma River).
[b] NW Germany: according to Diedrich (2009).

narrower medially than the left (20.4 and 23.4 mm, respectively). The spinous process of the middle vertebra is inclined to the left. In the places of fusion of the second and third sacral vertebrae asymmetric bone extensions are developed on either side. In general, the sacrum is slightly asymmetrical.

Caudal vertebrae (Fig. 6 B). Ten vertebra are present (F-2678/25-34).

Sternum bone (praesternum), F-2678/62 (Fig. 6C). The bone is complete, composed mainly of spongy bone tissue without an interval cavity. Approximately at a distance of a third of the bone

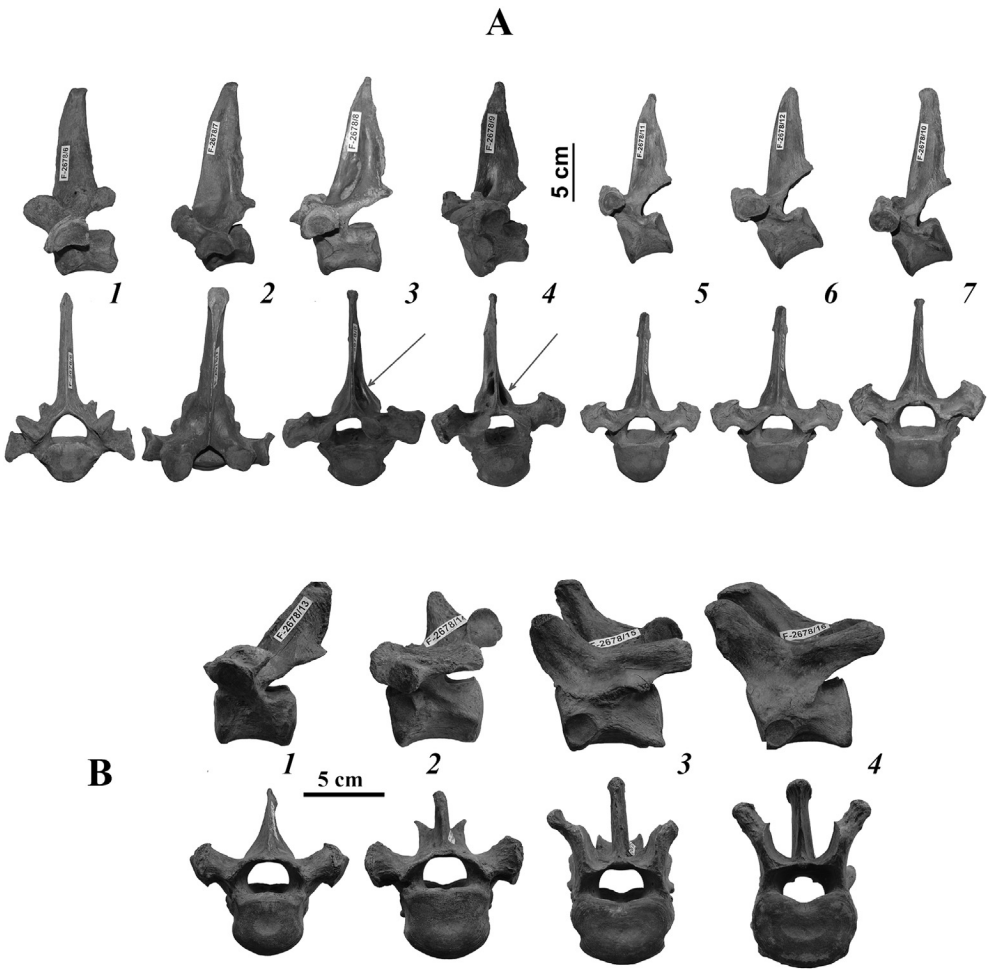

Fig. 4. Thoracic vertebrae of the Anyui lion. A: anterothoracic. Top — lateral view; bottom — anterior view, except no. 2 (upper view). Note the asymmetry of the vertebrae. The arrow points to the spinous process deformities (nos. 3 and 4). 1 — I (F-2678/6); 2 — II (F-2678/7); 3 — III (F-2678/8); 4 — IY (F-2678/9); 5 — Y (F-2678/11); 6 — YI (F-2678/11); 7 — YII (F-2678/12). Posterothoracic vertebrae of the Anyui lion. Top — lateral view; bottom —anterior view.1 — X (F-2678/13); 2 —XI (F-2678/14); 3 — XII (F-2678/15); 4 — XII (F-2678/16). Ice Age Museum.

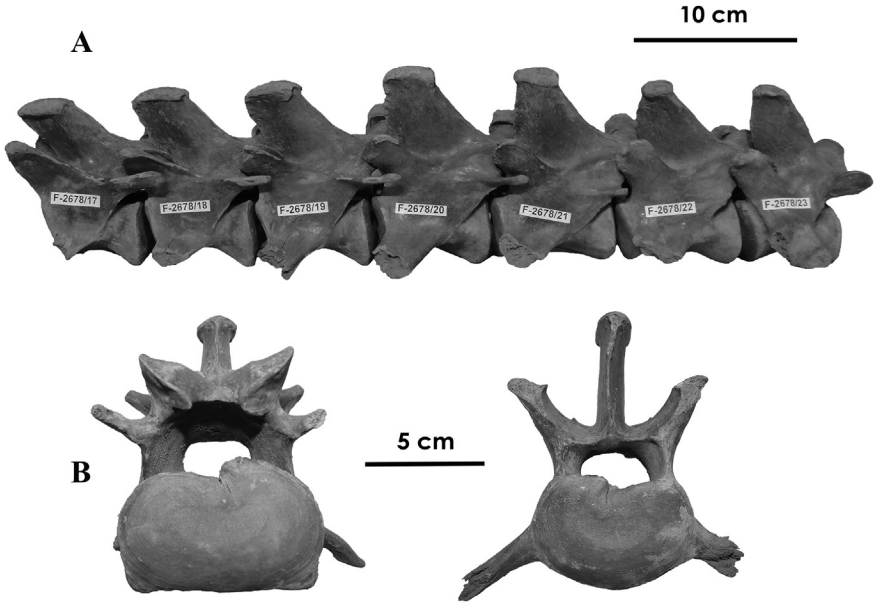

Fig. 5. Lumbar vertebrae of the Anyui lion. A — lateral view. B — 2nd and 3rd lumbar vertebrae, posterior and anterior views, respectively (Note the asymmetry of the vertebrae). SpecimensF-2678/17–23. Ice Age Museum.

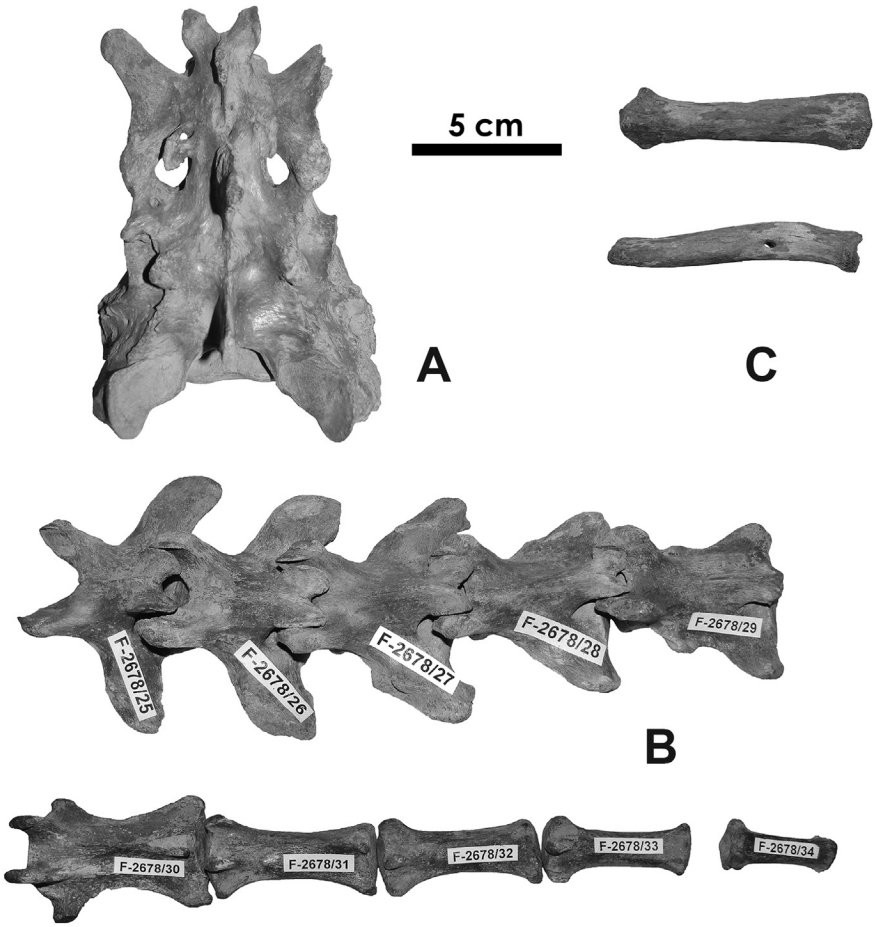

Fig. 6. Sacrum (A), caudalvertebrae (B) and sternum (C) of the Anyui lion. Specimens F-2678/24, F-2678/25-34 andF-2678/62. Ice Age Museum.

length, there is a large perforation 2.8–3.4 mm in diameter, which could have resulted from extreme extension of a vessel foramen.

Ribs, F-2678/35-54 (Fig. 7). Twenty ribs are present, including 11 left and 9 right ribs (complete bones and fragments). Some bones show age-related changes. For instance, the compact bone in the proximal region of two ribs (F-2678/50, 54) shows signs of bone loss, and small osteophytes are formed on six ribs (F-2678/37,/38,/40,/45,/47,/48).

4.1.2. Peripheral skeleton

Scapula, F-2678/55, dex. (Fig. 8A). The bone is complete, with osteophytes on its lower ridge. The ligament attachment facets are well developed. In the caudal region of the scapula base there is a prominent depression 70.7 mm long and 19 mm wide as measured medially (Fig. 8A, inset). The edges of the depression are thickened. The widened region of the distal ridge of the shoulder bone is uneven, with a natural depression 13.8 × 7.9 mm in size and 4.6 mm deep. Medially, the craniodorsal region of the shoulder bone has two well-developed bone ridges (where ligaments were attached), crossing each other at the right angle. The proximal region of the bone shows enlarged foramina; the largest (9.8 × 5.1 mm, and 7.3 mm deep), lies on the lateral side 61 mm from the articular facet edge. Two small foramina are located on the medial side, 50.3 mm from the edge of the facet. The larger of the two is 5.2 mm in diameter and 3.4 mm deep.

Humerus, F-2678/56, right (Fig. 8B). The bone is complete. The epiphyses were fused a long time ago, so the suture at their contact with the diaphysis is only noticeable in some proximal areas. The tubercles are well-developed at points of ligament attachment, especially on the lateral surface below the proximal epiphysis.

Pelvis (os coxae), F-2678/57, right side (Fig. 9A). The bone is complete. The obturator foramen is oval, slightly tapering anteriorly and wide posteriorly. The bone surface possesses distinct tubercles at the ligament attachment sites, especially around the acetabulum. During the animal's life the right and the left pelvic bones were fused, but were separated post mortem almost along the symphysis, while the pubic bone and the ischium were damaged in the contact zone.

Pelvis (os coxae), F-2678/58, left side (Fig. 9A). The bone is damaged.

Femur, F-2678/59, right (Fig. 9D). The bone is complete, compact and very dense, with undisturbed structural integrity, and no traces of bone loss. The ligament attachment sites on the posterior surface of the diaphysis are very prominent. Sclerotized ligaments are present within the acetabulum. A dense compact bone with a notch (ossified ligament) is observed immediately above the ectocondyle.

Tibia, F-2678/60, right (Fig. 9B). The diaphysis is strongly compressed laterally especially in the proximal region, where it is subtriangular in cross-section; with a narrow base of the posterior surface. The apical region protrudes considerably anteriorly. The tubercles at the ligament attachment sites are well-developed, especially proximally. Proximally, a denser area of compact bone 39.1 × 15.2 mm in size is visible. An osteophyte was formed beneath the proximal epiphysis (produced by a sclerotized ligament).

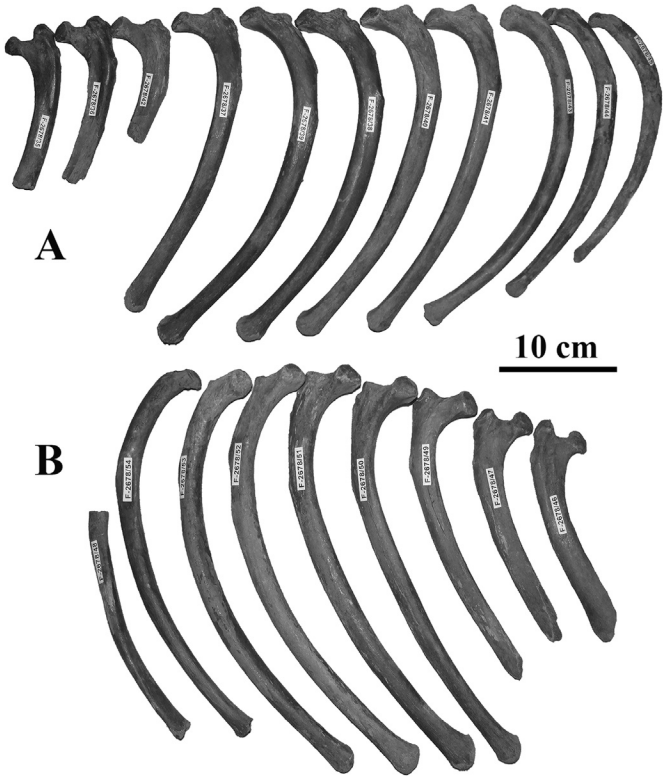

Fig. 7. Ribs of the Anyui lion. A — left; B — right. Specimens F-2678/35-54. Ice Age Museum.

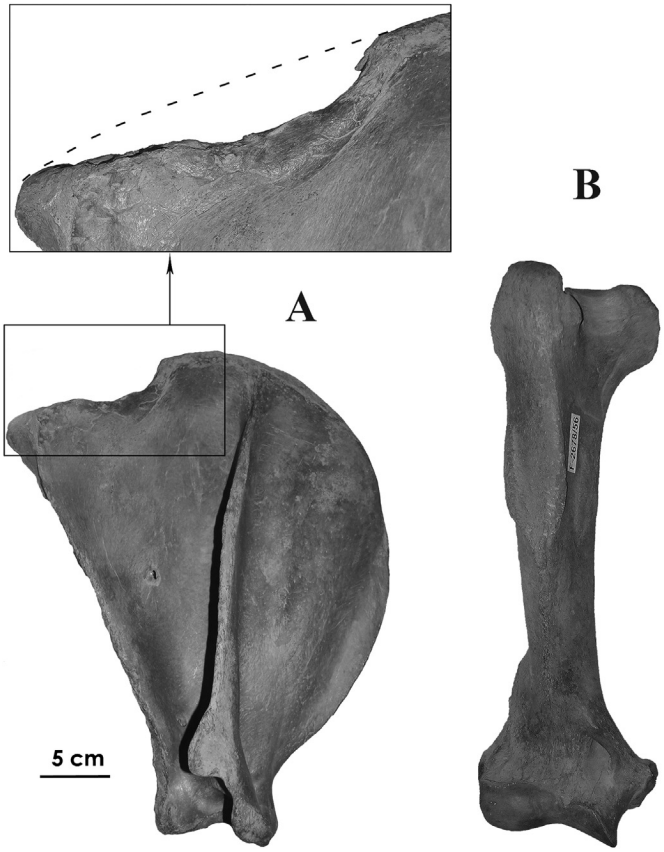

Fig. 8. Anterior limb bones of the Anyui lion. A — scapula, specimen F-2678/55; magnification in the frame: possibly an injury-related notch. B — humerus, specimenF-2678/56. Ice Age Museum.

Fibula, F-2678/61, right (Fig. 9C). The microrelief is prominent, especially in the ligament attachment sites. The lateral facets of the bone are sharp. A few osteophytes are present, the largest of these being in the proximal region.

Patellas, F-2678/64 and **F-2678/65** (Fig. 10A, B). Both patellas are oval with a cape-like elongated lower surface, weakly flattened. The articular facet of the bone is subquadrate, convex medially, with two wide facets facing the lateral sides of the bone. The anterior surface is considerably uneven in the ligament attachment sites.

Astragal, F-2678/63, right, and **Metatarsal III, F-2678/67**, left (Fig. 10C, D) have perfect preservation.

The third (claw) phalanx, F-2678/66 (Fig. 10 E). The surface is well preserved (Fig. 10, E-2), the inner surface and the base are partly missing. Regular annulations (transverse ridges of various sizes) are well developed.

A small bundle of hair, F-2678/70 (Fig. 10 F) about 4 g of weight is of a reddish color and contains guard hair and underfur of four and two size orders, respectively. The hair bundle is mainly represented by a thick underfur of numerous tightly packed and matted wavy fur hairs, which are not known in the extant lion (*Panthera leo*). This down hair, apart from insulating, regulated the thickness of the underfur and its air layer by to its compression and straightening, and also because of the developed medulla served as an effective insulator (Kirillova et al., 2014). A detailed description of this fur find as well as additional analyses will be given elsewhere.

4.2. One or two individuals of cave lion?

The lower jaw was found in the same place as the skeleton, but a year later, so it needed to be confirmed that it could belong to the same specimen. To determine whether or not the bones and mandibles belong to the same or different individuals, we analyzed the skeletal and cranial remains against several criteria, including sex, age, nature and degree of epigenetic changes, and individual features presented in Table 4. Taking into account that these parameters gave results that were all similar (or the same), it is highly probable that these remains belonged to a single individual.

Geneticists in possible future studies, which were beyond the scope of this paper, may be able to confirm (or reject) the results of the morphological study, and also to determine to which predator the hair might have belonged to.

4.3. Age and sex of the individual

All skeletal bones have similar age features: epiphyses are long fused with diaphysis; sutures absent or weak. The tissue of the bone surface is “mature”, “healthy” (i.e. even, dense, and smooth, without knobby projections, reflecting intensive metabolism). Neither is it scalloped, showing desorption of the bone tissue (found in aged and sick animals). Some bones have osteophytes, but showing no clear signs of bone tissue degeneration. The pelvic bones are fused, although not with the sacral vertebrae. All this indicates a mature, but not old animal.

The mandibles are not fused. The permanent premolars are worn off, the canine cusp is blunt, the pulp chamber is closed apically; the compact bone of the lower jaw is “mature”, fully formed; the ligament attachment sites are well developed. All these features indicate mature age.

The dating of the canines is based on the layers in the cross-section in the cement of the root. However, the thin section and the polished section clearly show only the external layers. Inner

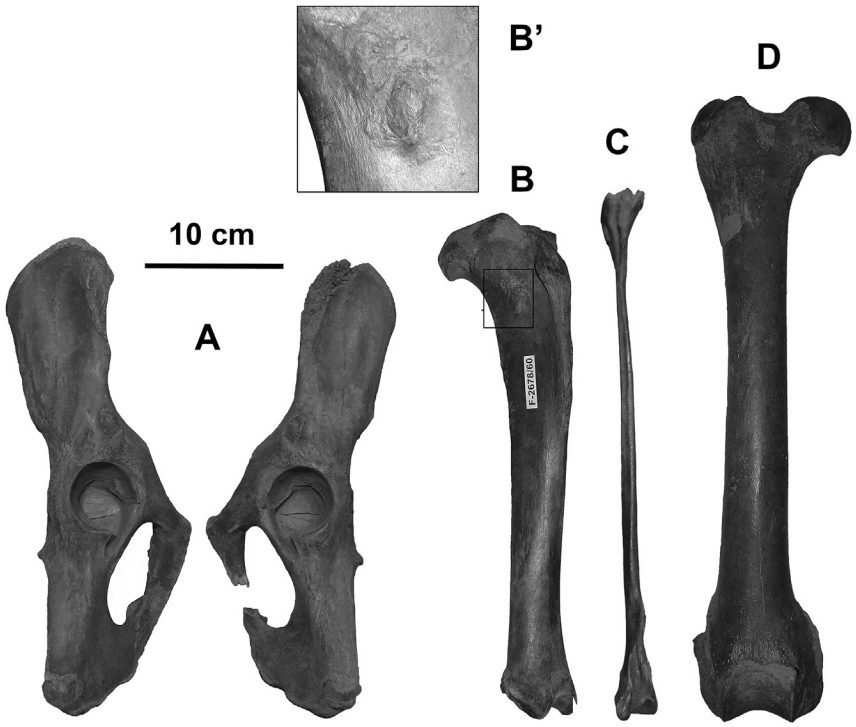

Fig. 9. Large bones of the posterior limbs of the Anyui lion. A — pelvis, F-2678/57-58; B — right tibia, F-2678/60 (B' — enlarged fragment with a surface osteoma); C — right fibula, F-2678/61; D — femur, F — 2678/59. Ice Age Museum.

layers, adjacent to the dentin, are diagenetically changed and cannot be analyzed. Such changes are characteristic of repeated thawing and freezing. The sagittal section distinctly shows cement with annual layers, dentin and secondary dentin at an early stage of formation. The cement is thicker on the inner side. There are 8 layers of the annular growth of cement, determined at a distance of 25 mm from the root apex, with reliability of four out of five in a scale of one to five. It is known that the annual layers of cement are first deposited as soon as the root dentin is formed. The deposition ceases if the root is exposed beyond the alveolar margin and its

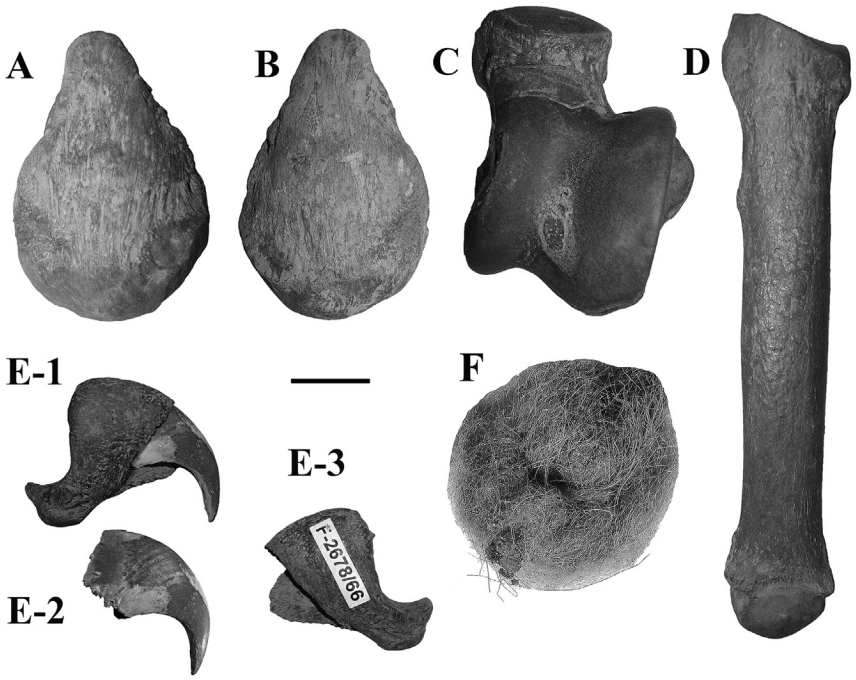

Fig. 10. Small bones of the posterior limbs of the Anyui lion and keratin skin derivates. A — right patella, F-2678/64; B — left patella, F-2678/65; C —right astragalus, F-2678/63; D — 3rd metatarsal (MtIII), F-2678/67. E — claw phalanx, F-2678/66: E-1 — complete; E-2 — claw sheath; E-3 — bone of the 3rd phalanx; F — mat of hair. Scale: 2 cm. Ice Age Museum.

Table 4
Criteria for assessing conformity of the cave lion skeletal and cranial remains from the Malyi Anyui River to a single individual.

Criteria for evaluation	Bones of skeleton F-2678/1-67	Mandibles F-2678/68-69
Individual age according to the state of dental and skeletal systems	Mature	Mature
Size class	Large	Large
Sex	Male	Male
Individual features	The asymmetry of the neural arch and spinal process of thoracic and other vertebrae resulted from an injury at an early age. The enlarged foramina on the neural arch and spinal process possibly resulted from an age-related hormonal change. The osteophyte beneath the proximal epiphysis on the tibia and the ligament ossifications on the femur and tibia resulted from an injury or increased functional load	Increased density of the compact bone is a result of an injury and increased load on the teeth. Expanded feeding foramina at the base of the tooth rows are likely to be product of an age-related hormonal change

nutrition is interrupted. The dentin walls of the root develop gradually, by adding annular layers in the growth zone in the lower root. The earlier layers are located closer to the cup. The apical foramen in extant big cats is closed at the age of 2.5–3 years (Yudin and Yudina, 2009). Later, the root cavity is gradually filled with dentin. The replacement of deciduous canines with permanent canines in big cats is complete by the age of one year. At that time, the canine is mainly composed of an enamel cusp and unformed root. The later annual growth in length of the root is reflected in the development of surface annulations clearly visible in young animals and is much less conspicuous in adults, because they are covered by many layers of cement. Such observations have been made for bear canines (Rausch, 1961; Klevezal et al., 2006) and apply to large predators in general. In our case, several of the earliest stages of the annual growth in the cement layers above the level where we counted the layers (25 mm from the root) are not observed. Judging from the visible transverse annulations, there were at least three stages. One more year needs to be added for the replacement of the deciduous canine with a permanent one (the stage when the tooth was represented only by an enamel cusp, with no root). Thus, the age of the animal at the time of its death was about 12 years.

The season of death of a large predatory mammal can be determined based on the last layer of cement in the teeth (Klevezal, 1988, 2007) and theoretically on the last layers in the claw sheath. Unfortunately, the season of death of the Anyui lion cannot be determined based on the cement of the canine, as this is not sufficiently well preserved, and neither is the proximal edge of the claw sheath.

Males of extant lions are usually 20–30% larger than females. Sexual dimorphism is also recorded for cave lions, where the criteria of sex determination are based on the size and proportions of various parts of the skeleton (Turner, 1984; Baryshnikov and Boeskorov, 2001; Diedrich, 2009, 2011a,b,c,d; Diedrich and Rathgeber, 2011). According to the accepted ratios: the length of the humerus to the width of its distal end; the length of the femur to the width of its distal end; the length of the tibia to the width of its distal end (Diedrich, 2011d), the skeleton from the Malyi Anyui River was a male. Large size and massive mandibles also suggest a male.

4.4. Size comparison

The humerus of the set found is almost identical in size to another occurrence of cave lion bones in Western Chukotka, from the Omolon River, Western Chukotka, housed kept in a private collection (Table 4). According to the measurements of cranial and skeleton elements given by various authors (Vereshchagin, 1971; Kurten, 1985; Argant, 1988; Diedrich, 2009, 2011a,b,c,d; Boeskorov et al., 2012), the Anyui Lion corresponds in size to other finds from N–E Russia (however, exceeding the size of the Late Pleistocene lions and more conforming to Middle Pleistocene ones). It was larger than East Beringian lions but smaller then West European ones (Tables 2 and 3).

4.5. Absolute age determinations

Results of radiocarbon measurements are summarized in Table 5.

Stable isotope measurements, done in the course of sample preparation and radiocarbon determinations are discussed in the following section. $\delta^{13}C$ values in Table 5 relate solely to the graphite targets used for the radiocarbon measurement and used only for fractionation correction of radiocarbon results. They can be slightly different from the parent material due to small isotopic fraction possible in graphite target preparation steps.

4.6. Isotope study

The analysis of collagen of the cave lion remains (coll. F-2678) showed that the samples fall into two groups. Samples F-2678/48, F-2678/118, F-2678/119 and F-2678/120 have almost identical isotope composition of collagen, suggesting that they almost certainly belonged to the same individual (Table 1). However, collagen of the lower jaw of the cave lion F-2678/69 is enriched in ^{13}C by 0.7‰, and depleted in ^{15}N by 1.1‰ (Fig. 11).

The mean $\delta^{15}N$ value of the four F-2678 collagen samples (+12.53‰) was slightly above those of the hair and claw samples (12.08 and 11.70‰, respectively). In contrast, $\delta^{13}C$ values in hair and claw (−21.36 and −21.25‰, respectively) were ca 1.4% lower than in the bone collagen (−19.90‰).

The isotopic signature of F-2678 collagen samples (including F-2678/69) was very similar to that of most other cave lions from western Chukotka and eastern Yakutia analyzed in this study. Two other large carnivorous mammals, *U. arctos* and *Canis* sp. (presumably *C. lupus*) had similar $\delta^{13}C$ and $\delta^{15}N$ values, though *Canis* sp. were often less enriched in ^{13}C and ^{15}N (Fig. 11).

To reconstruct the potential range of prey of the cave lion, we used an isotopic fractionation range previously established by Bocherens and Drucker (2003) between the collagen of prey and predator, i.e. from +0.8‰ to +1.3‰ and from +3‰ to +5‰ for $\delta^{13}C$ and $\delta^{15}N$, respectively. On the isotopic biplot, this calculation produces a rectangle that indicates average isotopic values of potential prey species (Bocherens et al., 2011).

The reconstructed range of the isotopic values of potential prey fell nearly exactly in the middle of average isotopic values of large ungulates, overlapping with the standard deviation of horses, bison, Ovibovini, *Ovis nivicola* and *Coelodonta*. Remarkably, reindeer and mammoths appear to be outside of the isotopic range of regular prey species (Fig. 12).

Table 5
Absolute dating of cave lion remnants from Malyi Anuyi River.

	ANSTO code	Sample type	Submitter ID	$\delta^{13}C$ per mil	Percent modern carbon		Conventional radiocarbon age	
					pMC	1σ error	yrs BP	1σ error
1	OZQ290	Bone	S-2-F-2678/48	−19.6 ± 0.2	0.02	±0.01	>61,000	
2	OZQ291	Claw	S-3-F-2678/66	−20.6 ± 0.2	0.00	±0.01	NDFB[a]	
3	OZQ292	Hair and wool	S-4-F-2678/70	−19.5 ± 0.2	2.81	±0.05	28,690	±130

[a] Not Distinguishable From Background (NDFB).

5. Discussion

Cave lion remains, including complete skeletons, are relatively abundant in the western regions of its range (Vereshchagin, 1971; Kurtén, 1985; Diedrich, 2011a,b,c,d), primarily in caves. In Russia, cave lion remains are less common, mainly disassociated bones. Associated occurrences are rare, for instance skeletons of digits from the Avdeevo site on the Russian Plain (Gvozdover, 2001). The discovery of the skeleton from the Malyi Anyui River contributes information on regional features of this species. The measurements of the mandible and skeletal bones on a first glance correspond to those of cave lion from N–E Russia (Tables 2 and 3). However, determination of its systematic position demands independent genetic studies, as well as a detailed comparison with other finds from different regions.

5.1. Geological age

Loose sediments, composing the accumulative surface on the right bank of the Malyi Anyui River at the cave lion skeleton locality site are Late Pleistocene in age. The radiocarbon age of the lion remains exceeds 61,000 years, which is older than previously known for this site. This could mean that the river exposed older beds at the base of the Krasivoe Section. The river valley expands eastward due to lateral erosion and cuts through the Pleistocene deposits that compose the right bank, causing lateral asymmetry of the river valley. However, the intensive meandering of the river in the lower reaches of the plain often leads to meandering and exposing of older beds.

5.2. AMS-radiocarbon dating

The ages are presented following the M. Stuiver and A. Polach (1977) convention. Bone and claw samples agree between each other and demonstrate the great antiquity of the studied specimen beyond the range of the radiocarbon method, with claw keratin found not distinguishable from background (NDFB). The hair sample on the other hand produced a much younger date arguing for its origin from a different individual. However, noting that the studied hair/wool strands exhibited a well-developed medulla, one may comment that the employed hair cleaning protocol after O'Connell and Hedges (1999) would not be able to fully remove possible contamination trapped in medulla voids. This in theory could explain a younger date for the hair sample still leaving some possibility for it to be associated with the discovered skeleton. Further investigations with more rigorous hair cleaning protocols are planned.

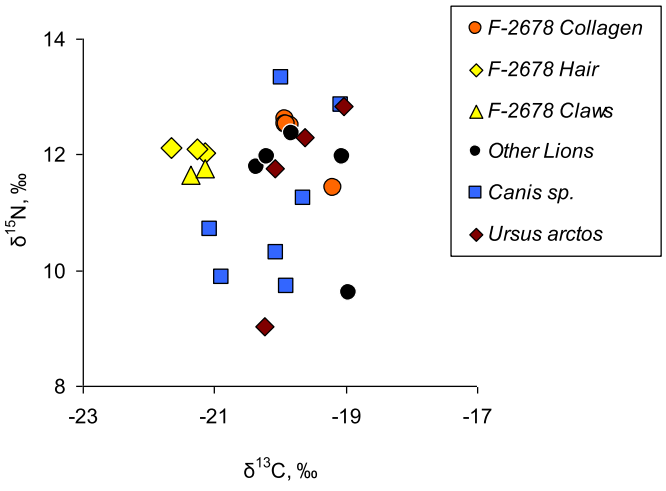

Fig. 11. Isotopic composition ($\delta^{13}C$ and $\delta^{15}N$ values) of bone collagen, hair and claw of *P. spelaea* specimen F-2678 (note a dissimilar signature of the F-2678/69 sample). Isotopic composition of bone collagen of other large predators is given for comparison.

5.3. Discussion of the isotope study and diet

Four out of five F-2678 collagen samples had remarkably similar isotopic composition. Mean $\delta^{13}C$ value of these samples is within the range of $\delta^{13}C$ values of Beringian cave lions (from −20.3 to −17.6‰) reported in Barnett et al. (2009). The $\delta^{15}N$ value of the Malyi Anyui River specimen is close to the upper limit of previously reported $\delta^{15}N$ values for Beringian lions (from 5.4 to 12.5‰). Noteworthy, the highest $\delta^{15}N$ values (above 11‰) were reported from Yakutia and western Chukotka (Barnett et al., 2009). Relatively

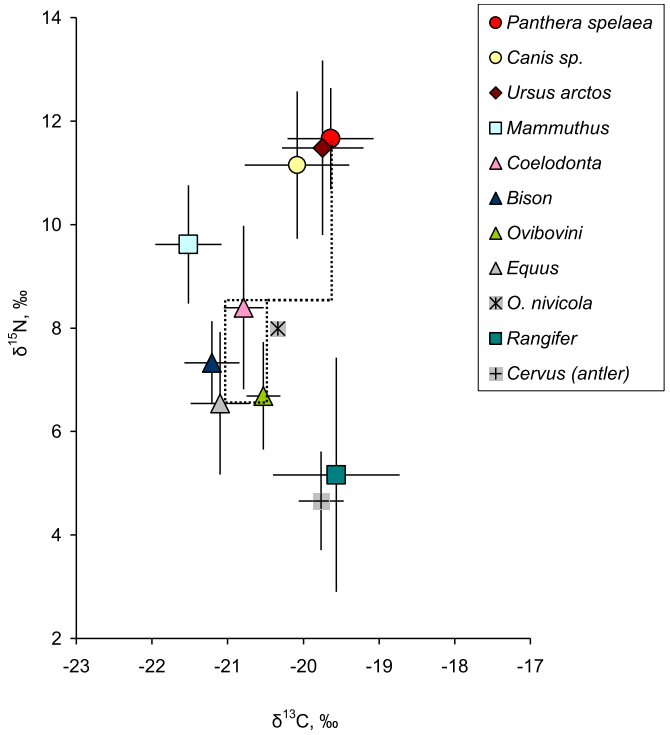

Fig. 12. Mean (±1 SD, $n = 7$) $\delta^{13}C$ and $\delta^{15}N$ values of bone collagen of *P. spelaea* from western Chukotka and northeastern Yakutia, other large predators and herbivores (samples from the Ice Age Museum collection). Potential prey species of *P. spelaea* (dashed rectangle) are suggested according to Bocherens and Drucker (2003).

high $\delta^{15}N$ values were also recognized in herbivores (Fig. 13), and are evidently typical of the animal in this region in the Late Pleistocene. It is very possible that these values correspond to cooler and drier conditions compared to other regions (Szpak et al., 2010).

The left mandible F-2678/69 had slightly different $\delta^{13}C$ and $\delta^{15}N$ values (Fig. 11). The difference is, apparently, outside the expected intra-individual dispersion. On the other hand, the mandible was affected by pathological deformation (see below) and this could lead to deviations in the isotopic composition of collagen (Katzenberg and Lovell, 1999).

The difference between the mean value of $\delta^{13}C$ in the bone collagen of the cave lion F-2678 and in the sample of hair and claw was 1.4‰, which approximately corresponds to the usual difference in this value between the hair and bone collagen in mammals (Bocherens et al., 2014). The identity of $\delta^{13}C$ and $\delta^{15}N$ values in fur and claw also suggests that these keratin skin derivatives belonged to the same species. Nevertheless, a similar isotopic composition of different individuals of the cave lion and that of other predators (Fig. 11) does not allow an unequivocal assignment of the fur to the individual F-2678.

The reconstruction of the potential diet of the cave lion using the isotope analysis, suggests that the diet consisted mainly of large ungulates (*Bison*, *Ovis*, *Ovibovini*, *Coelodonta* and *Equus*) (Fig. 12). However, two considerations are noteworthy. Firstly, the isotope analysis can unambiguously determine the food object only when the isotopic composition of the food object is original and is on the margin of the "isotopic field" of potential prey (Bocherens et al., 2011). In this case several food objects were exactly in the center of the isotopic field. Hence, the lion from the Malyi Anuy River could have fed on all the above kinds of ungulates.

It is known than cave lions had individual dietary preferences. For instance, in some regions of Western Europe they specialized on suckling cave bears cubs and reindeer (Bocherens et al., 2011; Diedrich, 2011d); and the dietary habits of the cave lions of Eastern Beringia were reconstructed (Fox-Dobbs et al., 2008). However, the relatively low range of $\delta^{13}C$ and $\delta^{15}N$ values in our sample of cave lions from northeastern Russia apparently indicates that their diet was more or less uniform. The exception is sample F-2450 (female), with $\delta^{15}N$ values 2–2.5‰ lower than other individuals (Fig. 11).

The trophic enrichment factor in bone collagen is on average +3.8‰ for $\delta^{15}N$ (Bocherens et al., 2015). Using original and published data (Bocherens et al., 1995, 1996, 2011, 2015; Fox-Dobbs et al., 2008), we compared $\delta^{15}N$ values in cave lions and potential prey species in different regions (Fig. 13A). This analysis suggests that *P. spelaea* could feed on *Bison*, *Ovis*, *Equus*, and *Rangifer*, whereas regular feeding on mammoth (which typically have very high $\delta^{15}N$ values) was not likely. On the other hand, the trophic enrichment factor for $\delta^{13}C$ is about +1.1‰. The analysis of $\delta^{13}C$ values in *P. spelaea* and potential prey species (Fig. 13B) confirms that the reindeer were not usual prey in most of regions, because their $\delta^{13}C$ values were often similar to that of cave lions. The expected trophic enrichment in ^{13}C between reindeer and lion was observed in two cases from the Western Europe only (Bocherens et al., 2011). Judging from Fig. 13B, the most likely prey of the cave lion could in most cases be *Bison*, and to a lesser extent *Equus*. Samples from Yakutia (Bocherens et al., 1996) do not support this conclusion, but it should be noted that in the above study bison and lion were represented by a single specimen each, and the samples were widely separated geographically. Modern African lions can obtain any prey, from warthogs to adult elephants, depending on choice. Collective hunting is often a condition for success. The choice of prey is certainly determined by the size and abundance of the prey, rather than by its taste. A small proportion of reindeer in the diet of the cave lion from northeastern Asia most likely suggests a low abundance of that species in this geographic region at that time. Indeed, the proportion of reindeer bones among other ancient ones from the frozen sediments is low.

5.4. Individual age

The presence of sclerotized ligaments on the shoulder, hip, and shin bones suggests high strain (possibly, the cause of myositis) and constant, springy movements of the paws.

In studying predators, the individual age can be determined from a canine: the first layers of cement do not reach the root apex, whereas the apical region of the root has only the latest layers of cement, which do not reach the base of the crown. Thus, if we assume that in the first year of life after the appearance of the enamel cusp, the root grows to reach half of its full (subsequent) length,

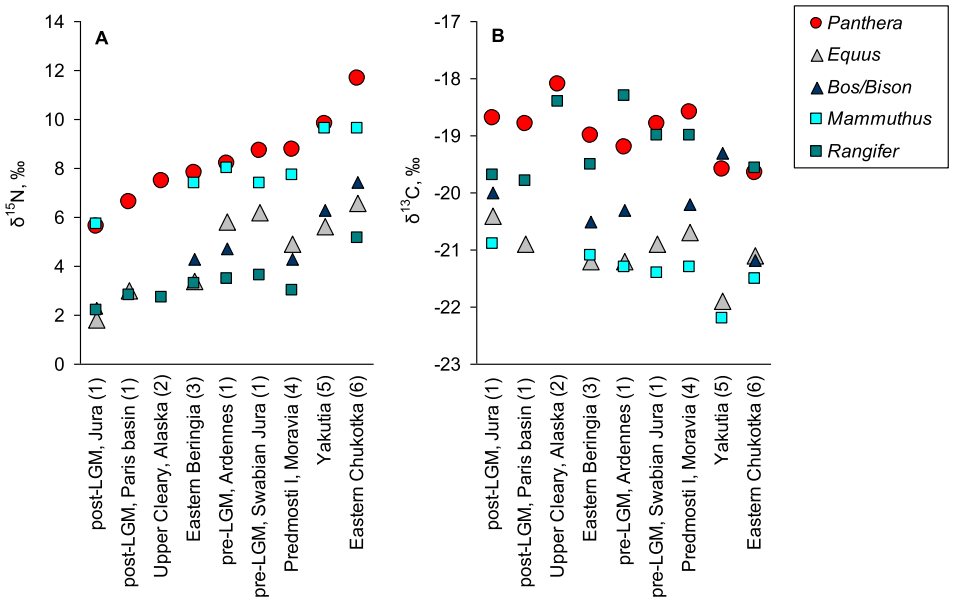

Fig. 13. Mean $\delta^{15}N$ (A) and $\delta^{13}C$ (B) values of bone collagen of *Panthera* spp. (mostly *P. spelaea*) and large herbivores according to published data. (1) Bocherens et al. (2011); (2) Bocherens et al. (1995); (3) Fox-Dobbs et al. (2008); (4) Bocherens et al. (2015); (5) Bocherens et al. (1996); (6) this study.

nothing should be added to determine the age. However, we have no such data. Therefore, for predators, the middle part of the root is usually examined for age determination. It is possible that about 1–2 layers of the first years of life are not included, but no more than that.

With some exceptions (e.g. a lion in the Serengeti that lived for 18 years) extant male lions live up to 10–12 years in the wild. This was an approximate life span of the Anyui cave lion. The growth of the claw sheath is expressed as transverse annulations of two size classes: distinct large and less distinct small ridges (Fig. 10E-2). It is noteworthy that although lions, like other cats, retract the claws into skin sockets near the digital pads when they move (keep them permanently retracted), lions file them off the bodies of their prey. However, regular replacement of the claw sheaths is important; for example Amur tigers in captivity replace the sheaths about three times a year as the tips become blunt (Yudin and Yudina, 2009). For the other large feline, the mountain lion, the growth rate of the claws was shown to be so high (Henaux et al., 2011), that it is not even remotely possible to correlate the annulations on the claw sheaths with the years of life. The same applies to the claw of the Anyui lion. Its record can only be used for the period immediately preceding death. It is possible to determine the exact number of growth increments. The affinity of three large ridges in the center of the claw is difficult to assess. They are morphologically conspicuous, but it is not clear whether they represent annual increments. Smaller rhythms are also present. Domestic cats shed their claws on regular basis, and rapidly replace them. It is possible that the Anyui lion died while still replacing claws.

5.5. Individual features and pathologies of the skeleton

Some skeletal elements of the Malyi Anyui cave lion have variously expressed morphological deviations. These include the lower jaw, several thoracic vertebrae, the sacrum, and the scapula.

Morphological features of the left mandible are well observed on a radiograph. The mandible bone is denser on the lingual side of the mandible, including the central region near the anterior teeth and near p4 and m1where the buccal compact bone is the densest (Fig. 2B). Most likely these are caused by an injury leading to the development of periostitis. The buccal teeth of the cave lion have a large cusp and root, which suggests that they can resist considerable strain. The development of the root cement also reveals strain. The more strain, the thicker the cement. The thickness of the cement is indeed very considerable. Furthermore, the microrelief of the root surface periphery is evenly wavy (Fig. 2E). Apparently, such a structure is an additional adaptation to high strain, which was compensated by an increase of the attachment area. It would be interesting to test this hypothesis on cross-sections of teeth of modern lions, but unfortunately we do not have such material at our disposal.

V.G. Yudin's observations of Amur tigers in captivity showed that the tigers, when food is abundant, try to eat only the flesh, possibly to preserve their teeth, whereas bears eat the flesh together with the bones. However, in the wild tigers usually eat their prey completely. If the Anyui lion gnawed the bones (which is more typical for bears and hyenas), this would certainly have been reflected in the state of its teeth. However, the lateral wear of the buccal teeth by the upper teeth shows similar feeding habits to the tiger. It is possible that the relatively good state of the teeth, taking into account the age of the animal, shows that it hunted its own prey (mainly eating soft tissues and to a lesser extent, frozen carcasses). The enlarged blood vessel foramina along the dental rows and flaking of the compact bone on the external side of the dental bone (the early stage of the recurrent periostitis) observed on specimen F-2678/68-69 indicate hormonal changes in the animal. Hence these are more likely age-related rather than pathological changes resulting from an injury at an early age. The feature could also be determined genetically.

The canine is worn apically for about 5–7 mm. Wearing of the canines in large felines results from killing and tearing the prey. As mentioned above, the canine has a pronounced dent (Fig. 2D). Perhaps, this dent is a trace of an impact from a hard object (e.g., a fang of another large predator). A weak smoothening of the edges of the dent shows that the lion survived the injury.

The most striking morphological deviations are noted in the morphology of vertebrae (depressions on the neural arch and spinous process of the thoracic vertebrae; asymmetry of thoracic, lumbar, and sacral vertebra) and of the shoulder bone (uneven surface of the proximal side, with a dense compact bone). The morphological features of the three thoracic vertebrae are not unique. We noticed a similar morphology on the thoracic vertebrae of a mammoth (specimen F-300, from the Ice age Museum collection). Possibly, in this case the morphology reflects a disruption of normal cartilage-bone turnover, i.e., locally remained cartilage and locally underdeveloped bone. However this seems to be an individual or a genetically predisposed character, rather than a functional deformity.

The irregular surface of the shoulder bone could be a trace of an early age injury, or excessive development of the muscle attachment area, which could be damaged or shifted. Nevertheless, these deformities did not prevent the lion from surviving to a considerable age. Ossification of ligaments, present on the femur and tibia, is usually observed in very active animals, as result of significant strain, usually following myositis.

6. Conclusions

The find from the Malyi Anyui River represents the first associated skeletal remains of a cave lion in Russia. Its individual features, including the periostitis of the lower jaw, asymmetry of thoracic and sacral vertebrae, depression on the scapula, sclerotized ligaments on the femur and tibia are most likely related to an injury at an early age. It is possible that the animal had some problems with locomotion. In size, the skeletal elements are similar to those of other cave lion occurrences from northeastern Russia but are bigger than ones from East Beringia and smaller than from West Europe. According to the stable isotope signal, the fur found near the skeleton could belong to a cave lion. The considerable difference in the geochronological dating is interesting and needs further study, as well as systematic position and genetics. The cave lion of northeastern Russia has uniform food preferences. It is unlikely that reindeer formed an important part of its diet, which consisted largely of bison and horses, quite a different diet from that of Western European cave lions.

Acknowledgments

We are grateful to Leo Meskhe for the discovery of the cave lion skeleton and careful collection of the remains, to G.A. Klevezal for consultations, to N.I. Grechaninko for radiography, to M.G. Zhilin for trassological expertise, to N.A. Semenov and O.V. Krylovich for technical assistance, and to anonymous reviewers, whose valuable comments allowed improving the manuscript. The study was supported by the National Alliance of Shidlovskiy “Ice Age”. English language was checked by M.V.L. Barclay (Natural History Museum, London, UK).

References

Argant, A., 1988. Etude de l'exemplaire de *Panthera spelaea* (Goldfuss, 1810) (Mammalia, Carnivora, Felidae) du gisement Pleistocene moyen recent de la grotte d'Aze (Saone et Loire). Rev. Paleobiol. 7 (2), 449–466.

Arkhangelov, A.A., Konyakhin, M.A., 1978. Permafrost-facial Structure of the Riverbed Deposits of the Edomnaya Formation of the Kolyma Lowlands. In: Problemy Kriolitologii. Iss. 7. Moscow State University Press, Moscow, pp. 58–73 (in Russian).

Barnett, R., Shapiro, B., Barnes, I., Ho, S.Y.W., Burger, J., Yamaguchi, N., Higham, T.F.G., Wheeler, T., Rosendahl, W., Sher, A.V., Sotnikova, M., Kuznetsova, T., Baryshnikov, G.F., Martin, L.D., Harington, R., Burns, J.A., Cooper, A., 2009. Phylogeography of lions (*Panthera leo* ssp.) reveals three distinct taxa and a late Pleistocene reduction in genetic diversity. Mol. Ecol. 18, 1668–1677.

Baryshnikov, G., Boeskorov, G., 2001. The Pleistocene cave lion, *Panthera spelaea* (Carnivora, Felidae) from Yakutia, Russia. Cranium 18 (1), 7–23.

Bocherens, H., Drucker, D., 2003. Trophic level isotopic enrichments for carbon and nitrogen in collagen: case studies from recent and ancient terrestrial ecosystems. Int. J. Osteoarchaeol. 13, 46–53.

Bocherens, H., Emslie, S.D., Billiou, D., Mariotti, A., 1995. Stable isotopes (^{13}C, ^{15}N) and paleodiet of the giant short-faced bear (*Arctodus simus*). C. R. l'Acad. Sci. Paris 320, 779–784.

Bocherens, H., Pacaud, G., Lazarev, P., Mariotti, A., 1996. Stable isotope abundances (^{13}C, ^{15}N) in collagen and soft tissues from Pleistocene mammals from Yakutia. Implications for the paleo- biology of the mammoth steppe. Palaeogeogr. Palaeoclimatol. Palaeoecol. 126, 31–44.

Bocherens, H., Drucker, D.G., Bonjean, D., Bridault, A., Conard, N.J., Cupillard, Ch, Germonpre, M., Honeisen, M., Munzel, S.C., Napierala, H., Patou-Mathis, M., Stephan, E., Uerpmann, H.-P., Ziegler, R., 2011. Isotopic evidence for dietary ecology of cave lion (*Panthera spelaea*) in North-Western Europe: prey choice, competition and implications for extinction. Quat. Int. 245, 249–261.

Bocherens, H., Grandal-d'Anglade, A., Hobson, K.A., 2014. Pitfalls in comparing modern hair and fossil bone collagen C and N isotopic data to reconstruct ancient diets: a case study with cave bears (*Ursus spelaeus*). Isotopes Health Environ. Sci. 50, 291–299.

Bocherens, H., Drucker, D.G., Germonpré, M., Lázničková-Galetová, M., Naito, Y., Wissing, C., Brůžek, J., Oliva, M., 2015. Reconstruction of the Gravettian food-web at Předmostí I using multi-isotopic tracking (^{13}C, ^{15}N, ^{34}S) of bone collagen. Quat. Int. 359–360, 211–228.

Boeskorov, G.G., Belolubskiy, I.N., Plotnikov, V.V., Davidov, S.P., Lazarev, P.A., Orlova, L.A., Stepanov, A.D., Baryshnikov, G.F., 2012. New finds of fossil cave lion in Yakutia. Sci. Educ. 2, 45–51 (in Russian).

Bronk Ramsey, C., Higham, T., Bowles, A., Hedges, R., 2004. Improvements to the pretreatment of Bone at Oxford. Radiocarbon 46 (1), 155–163.

Brown, T.A., Nelson, D.E., Vogel, J.S., Southon, J.R., 1988. Improved collagen extraction by modified Longin method. Radiocarbon 30 (2), 171–177.

Diedrich, C.G., 2009. Upper Pleistocene *Panthera leo spelaea* (Goldfuss, 1810) remains from the Bilstein Caves (Sauerland Karst) and contribution to the steppe lion taphonomy, palaeobiology and sexual dimorphism. Ann. Paléontol. 95, 117–138.

Diedrich, C.G., 2011a. A diseased *Panthera leo spelaea* (Goldfuss 1810) lioness from a forest elephant graveyard in the Late Pleistocene (Eemian) interglacial lake at Neumark-Nord. Hist. Biol. 23, 195–217.

Diedrich, C.G., 2011b. Late Pleistocene *Panthera leo spelaea* (Goldfuss, 1810) skeletons from the Czech Republic (central Europe); their pathological cranial features and injuries resulting from intraspecific fights, conflicts with hyenas, and attacks on cave bears. Bull. Geosci. 86 (4), 817–840.

Diedrich, C.G., 2011c. Late Pleistocene steppe lion *Panthera leo spelaea* (Goldfuss, 1810) footprints and bone records from open air sites in northern Germany — evidence of hyena-lion antagonism and scavenging in Europe. Quat. Sci. Rev. 30, 1883–1906.

Diedrich, C.G., 2011d. The largest European lion *Panthera leo spelaea* (Goldfuss 1810) population from the Zoolithen Cave, Germany: specialized cave bear predators of Europe. Hist. Biol. 23 (2–3), 271–311.

Diedrich, C., Rathgeber, T., 2011. Late Pleistocene steppe lion *Panthera leo spelaea* (Goldfuss, 1810) skeleton remains of the Upper Rhine valley (SW Germany) and contribution to their palaeobiogeography, sexual dimorphism and habitus. Hist. Biol. 86, 1–28.

Fink, D., Hotchkis, M., Hua, Q., Jacobsen, G., Smith, A.M., Zoppi, U., Child, D., Mifsud, C., Gaast van der, H., Williams, A., Williams, M., 2004. The ANTARES AMS facility at ANSTO. NIM B 223–224, 109–115.

Fox-Dobbs, K., Leonard, J.A., Koch, P.L., 2008. Pleistocene megafauna from eastern Beringia: paleoecological and paleoenvironmental interpretations of stable carbon and nitrogen isotope and radiocarbon records. Palaeogeogr. Palaeoclimatol. Palaeoecol. 261, 30–46.

Gvozdover, M.D., 2001. Zooarchaeology of the Upper Paleolithic Avdeevo site. In: Mammoth and its Environments: 200 Years of Investigations. GEOS, Moscow, pp. 335–345 (in Russian).

Henaux, V., Powell, L.A., Hobson, K.A., Nielsen, C.K., LaRue, M.A., 2011. Tracking large carnivore dispersal using isotopic clues in claws: an application to cougars across the Great Plains. Methods Ecol. Evol. Br. Ecol. Soc.

Higham, T.F.G., Jacobi, R.M., Bronk Ramsey, C., 2006. AMS radiocarbon dating of ancient bone using ultrafiltration. Radiocarbon 48 (2), 179–195.

Hua, Q., Jacobsen, G.E., Zoppi, U., Lawson, E.M., Williams, A.A., Smith, A.M., McMann, M.J., 2001. Progress in radiocarbon target preparation at the ANTARES AMS Centre. Radiocarbon 43 (2a), 275–282.

Kaplina, T.N., Lakhtina, O.V., Abrashov, B.A., Koreisha, M.M., 1978. Criogenic Structure of the Late Pleistocene and Holocene Beds in the Valley of the Malyi Anyui River. Problemy Kriolitologii, Iss.7. Moscow University Press, Moscow, pp. 48–57 (in Russian).

Katzenberg, M.A., Lovell, N.C., 1999. Stable isotope variation in pathological bone. Int. J. Osteoarchaeol. 9, 316–324.

Kirillova, I.V., Chernova, O.F., Krylovich, O.V., Tiunov, A.V., Shidlovskiy, F.K., 2014. A discovery of a cave lion (*Panthera spelaea* Goldfuss, 1810) in Russia. Dokl. Biol. Sci. 455, 102–105.

Klevezal, G.A., 1988. Registriruyushchie Struktury Mlekopitayushchikh V Zoologicheskikh Issledovaniyakh (Recording structures of mammals in zoological investigations). Nauka, Moscow (in Russian).

Klevezal, G.A., 2007. Principles and Methods of Age Determination of Mammals. KMK Scientific Press Ltd., Moscow (in Russian).

Klevezal, G.A., Kirillova, I.V., Shishlina, N.I., Sokolov, A.A., Trunova (Selkova), YuE., 2006. Growth layers in tooth dentin and cementum: problems and perspectives of their use in the study of fossil and subfossil mammal remains including humans. Doc. Archaeobiol. 4, 113–124.

Konyakhin, M.N., Mikhalev, D.V., Solomatin, V.I., 1996. The Isotopic-oxygen Composition of the Subsurface Ice. Moscow University Press, Moscow (in Russian).

Kurtén, B., 1985. The Pleistocene lion of Beringia. Ann. Zool. Fenn. 22, 117–121.

Longin, R., 1971. New method of collagen extraction for radiocarbon dating. Nature 230, 241–242.

Lopez-Polin, Lucia, 2012. Possible interferences of some conservation treatments with subsequent studies on fossil bones: a conservator's overview. Quat. Int. 275, 120–127.

Mikhalev, D.V., 1990. I-oxygen Composition of the Texture-forming Ice (On an Example of the Kolyma Lowland and Northern Yenisei Region) (PhD thesis). Moscow University, p. 242.

Mikhalev, D.V., Nikolaev, V.I., Romanenko, F.A., Arkhipov, V.V., Brilli, M., 2006. Studies of key sections of perenially frozen rocks in the Lower Reaches of the Malyi Anyui River: preliminary results. In: Nikolaev, V.I. (Ed.), Stable Isotopes in Palaeoecological Studies, pp. 100–124 (in Russian).

Nikolaev, V.I., Mikhalev, D.V., Romanenko, F.A., Brilli, M., 2010. Reconstruction of the formation of perennial deposits in northeastern Russia based on the isotope study of the reference sections of the Kolyma Lowlands. Led. i Sneg 4 (112), 79–90 (in Russian).

O'Connell, T.C., Hedges, R.E.M., 1999. Isotopic comparison of hair and bone: archaeological analyses. J. Archaeol. Sci. 26, 661–665.

O'Connell, N.C., Hedges, R.E.M., 2001. Isotopic comparison of hair, nail and bone: modern analyses. J. Archaeol. Sci. 29, 1247–1255.

Rausch, R.L., 1961. Notes on the black bear *Ursus americanus* Pallas, in Alaska with particular reference to dentition and growth. Z. Säugetierkd. 26 (2), 77–107.

Sher, A., Plaht, I., 1988. Carbon dating and Pleistocene stratigraphy of the lowlands of the Northeastern USSR. Izvestiya Akademii Nauk SSSR. Seriya Geol. 8, 17–31 (in Russian).

Sotnikova, M., Nikolsky, P., 2006. Systematic position of the cave lion *Panthera spelaea* (Goldfuss) based on cranial and dental characters. Quat. Int. 142–143, 218–228.

Stuiver, M., Polach, A., 1977. Reporting of 14C data. Radiocarbon 19 (3), 355–363. Available on-line at: https://journals.uair.arizona.edu/index.php/radiocarbon/article/view/493/498.

Szpak, P., Gröcke, D.R., Debruyne, R., MacPhee, R.D.E., Guthrie, R.D., Froese, D., Zazula, G.D., Patterson, W.P., Poinar, H.N., 2010. Regional differences in bone collagen $\delta^{13}C$ and $\delta^{15}N$ of Pleistocene mammoths: implications for paleoecology of the mammoth steppe. Palaeogeogr. Palaeoclimatol. Palaeoecol. 286, 88–96.

Tomskaya, A.I., 1982. Palinostratigraphy of the Quaternary deposits of the Kolyma Lowlands. In: Stratigraphy and Palynology of the Sedimentary Deposits of Yakutia. Yakutsk Branch, Siberian Division, Russian Academy of Sciences, Yakutsk, pp. 100–101.

Turner, A., 1984. Dental sex dimorphism in European lions (*Panthera leo* L.) of the Upper Pleistocene: palaeoecological and palaeoethological implications. Ann. Zool. Fenn. 21, 1–8.

van Klinken, G.J., 1999. Bone collagen quality indicators for paleodietary and radiocarbon measurements. J. Archaeol. Sci. 26, 687–695.

Vereshschagin, N.K., 1971. The Cave Lion and its History in the Holarctic and on the Territory of the U.S.S.R, vol. 49. Trudy of Zoological Institute, Leningrad, pp. 123–199 (in Russian).

von den Driesch, A., 1976. The Measurement of Animal Bones from Archaeological Sites. Peabody Museum Bulletin 1. Peabody Museum of Archaeology and Etiology. Harvard University.

Yudin, V.G., Yudina, E.V., 2009. The Tiger of the Far East of Russia. Dalnauka, Vladivostok (in Russian).